

Annals of the University of Craiova

The Chemistry Series

Analele Universității din Craiova
Seria Chimie

Volume XLIV, no. 2

2017

Editor in Chief

Cezar Spînu University of Craiova

Co-Editors

Cristian Tigae University of Craiova

Paul Chiriță University of Craiova

Issue Editor

Bogdan Tutunaru University of Craiova

Editorial Board

Véronique Barragan-Montero - Université de Montpellier, France

Jean-Louis Montero - Université de Montpellier, France

Alain Fruchier- Ecole Nationale Supérieure de Chimie de Montpellier, France

Michel Schlegel – Commissariat a l'Energie Atomique (CEA)

Michael Descostes - Commissariat a l'Energie Atomique (CEA)

Ilea Petru - Babeş-Bolyai University, Cluj-Napoca

Anca Cojocaru - Politehnica University of Bucharest

Oana Stănaşel - University of Oradea

Cristina Băbeanu - University of Craiova

Aurora Reiss - University of Craiova

Mihaela Mureşeanu - University of Craiova

Simona Sbârna - University of Craiova

Bogdan Tutunaru - University of Craiova

Aurelian Dobriţescu - University of Craiova

Georgeta Ciobanu - University of Craiova

Anca Moanță - University of Craiova

Cătălina Ionescu - University of Craiova

Andreea Simionescu - University of Craiova

Contact

Phone: +40 251 597048

Fax: +40 251 597048

Web page: <http://chimie.ucv.ro/departament/>

e-mail: office@chimie.ucv.ro

Content

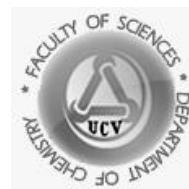
Research articles	
Use of NMR patterns in establishing the C- or O-alkylated structure in derivatives of protected mannose Cătălina Ionescu, Alain Fruchier, Georgeta Ciobanu, Anca Moanță, Véronique Barragan-Montero	2
Does the oxidation state impact chromium toxicity in wheat seedlings? Georgeta Ciobanu, Cătălina Ionescu, Aurora Reiss	12
Azoethers and azoesters with antimicrobial activity Anca Moanță, Cătălina Ionescu, Simona Iordache	24
Investigating the coordination manner of a heterocyclic thioamide to Pt(II) by EHT interpretation of the electronic spectra for both free and coordinated organic ligand Liana Simona Sbîrnă, Sebastian Sbîrnă, Anișoara Oubraham	36
Total phenolic content and antioxidant activity in leaves of six Salix genotypes Cristina Băbeanu, Ana Maria Dodocioiu	48
Thermal Analysis of some Binuclear Bioactive Complexes Derived from an Aromatic Dialdehyde and L-Tryptophan Florina Ciolan, Anca Gănescu	58
Natural sources used to obtain edible films Mihaela Gabriela Dumitru	65
The oxidative dissolution of iron monosulfide (FeS): A Cyclic Voltammetry study Mădălina Duinea, Maria Manea, Ana Sandu, Bianca Ghejan, Mihaela Petcu, Paul Chiriță	75
Synthesis and description of three square-planar d8 complex compounds involving charge-transfer systems Liana Simona Sbîrnă, Clementina Moldovan	82

Annals of the University of Craiova

The Chemistry Series

Volume XLIV, No. 2 (2017) 2-11

homepage: chimie.ucv.ro/anale/



Use of NMR patterns in establishing the C- or O-alkylated structure in derivatives of protected mannose

Research article

Cătălina Ionescu^{1,}, Alain Fruchier², Georgeta Ciobanu¹, Anca Moanță¹,
Véronique Barragan-Montero³*

¹University of Craiova, Faculty of Sciences, Department of Chemistry, Calea Bucuresti, 107i, Craiova, Romania

²UMR CNRS 5253—ENSCM, 8 rue de l'École Normale, 34296 Montpellier cedex 5, France

³Faculté des Sciences, CC 750, Faculté d'odontologie, Laboratoire de Bioingénierie et Nanosciences, 545 Avenue du Professeur Jean-Louis Viala, 34193 Montpellier cedex 5, France

*E-mail: catalinagurgui@yahoo.co.uk; jpschim@kunsan.ac.kr

Received: 24.11.2017 / Accepted: 13.12.2017 / Published: 22.12.2017

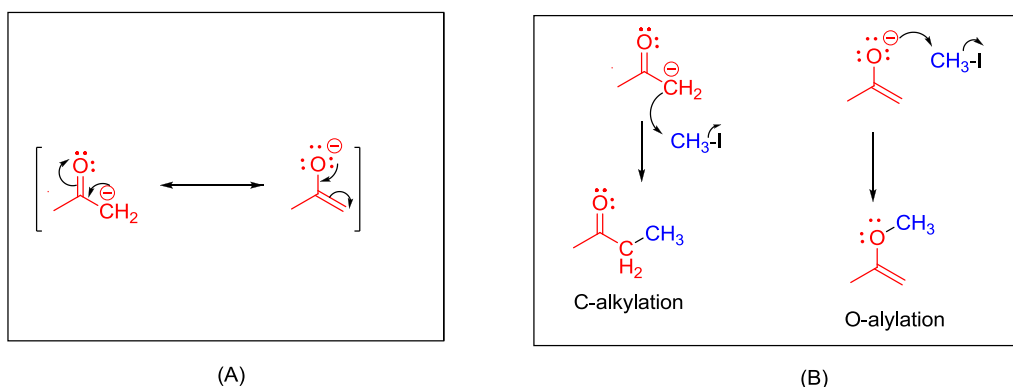
Abstract

Ambident nucleophiles can lead to isomers, therefore, it is important to know which of the centres has reacted. The anion of bis(2,2,2-trifluoroethyl) malonate (TFEM) can react either at oxygen, either at the methylene carbon atom. In a previous study, we have presented two alkylation reactions of protected mannose with TFEM via the Mitsunobu reaction at the anomeric and at the C6 position of the carbohydrate, leading to O-alkylated products or to mixtures of C- and O-alkylated products. In the present paper, the ¹H NMR patterns that allowed us to assign the chemical structures of the obtained products at the C6 position are detailed.

Keywords: ambident nucleophile, bis(2,2,2-trifluoroethyl) malonate, mannose, NMR

1. INTRODUCTION

Ambident nucleophiles are nucleophiles that can react at two different atoms in their structure, due to resonance stabilization of the negative charge over two atoms. The most well-known examples of ambident nucleophiles are enolates [1, 2] that can lead, through alkylation, either to C-alkylated (if the negative charge is localized at C), either to O-alkylated (if the negative charge is localized at O) compounds, or to mixtures of C and O-alkylated products (Scheme 1).



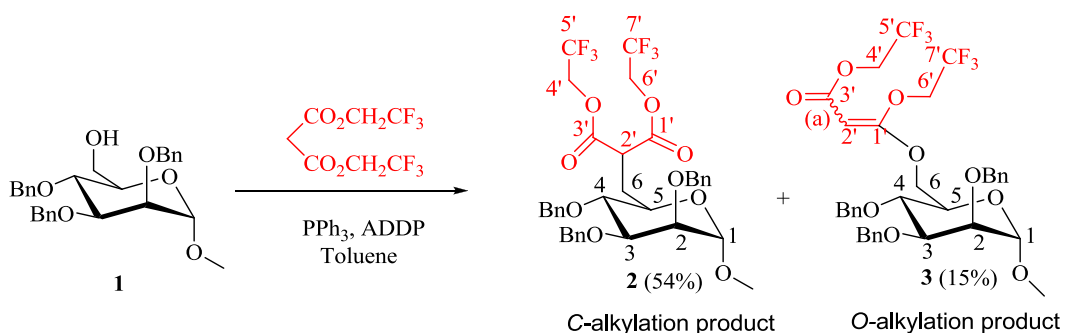
Scheme 1. Acetone enolate reactivity: (A) Resonance structures of acetone enolate; (B) C and O-alkylation of acetone enolate.

Other ambident nucleophiles exist, one of them being the anion of bis(2,2,2-trifluoroethyl) malonate (TFEM). In previous studies [3-5], we have used this double ester as reagent in the Mitsunobu reaction [6, 7] with appropriately protected mannose, having either the anomeric, or the C6 positions free for coupling. The results showed that, when applied to the anomeric position, only O-alkylated compounds have been identified, while at the C6 position, a mixture of C- and O-alkylated compounds has been obtained [4]. Many competitive alkylation reactions (e.g. N/O, N/S, C/O) under Mitsunobu conditions have been reported in literature, leading to sole reaction products or to mixtures of compounds [7-13]. In the mentioned papers, we have previously presented the structures and spectral data of the obtained products, with an emphasis on reaction mechanisms and possible explanations of the processes that lead to our results. In this study, we

are exposing the NMR data that allowed us to assign the C or O-alkylated structure to our products.

Because the Mitsunobu reaction of TFEM applied to the C6 position of protected mannose lead to both C- and O-alkylated products, we will use this reaction as case study. The structures of the two reaction products have been analysed using mass spectrometry and NMR spectroscopy. As the two products are isomers, mass spectrometry cannot easily assist in distinguishing between the two possible structures. In our study, differences have been noticed using NMR analyses: ^1H NMR and ^{13}C NMR. Other papers also describe NMR methods (HSQC/HMQC, HMBC, ROESY, and ^{13}C shift predictions) to differentiate between competitive alkylation products [14].

The reaction products detailed in this paper are obtained using the reaction described in Scheme 2.



Scheme 2. Reaction of protected mannose, free at C6 position, with TFEM, under Mitsunobu conditions [(a) the Z/E configuration has not been determined]

2. MATERIALS AND METHODS

2.1. Materials

The products (2 and 3) detailed in this paper have been obtained using the Mitsunobu reaction in conditions previously described [**Error! Bookmark not defined.**]. Products purification and spectral identification data of 2 and 3 are also contained in this publication.

2.2. Methods

Proton spectra have been recorded in CDCl₃ solutions on a Bruker DRX-400 spectrometer working at 400.13 MHz for ¹H and 100.62 MHz for ¹³C. ¹H-¹H and ¹H-¹³C correlation spectra were recorded with the standard pulse sequences.

3. RESULTS AND DISCUSSION

Among the spectral NMR data of compounds **2** and **3**, the patterns described in Table 1 allowed us to distinguish between the C- and O-alkylation products (**2** and **3**).

Table 1. Some NMR parameters of compounds **2** and **3** (chemical shifts δ in ppm; coupling constants J in Hz)

NMR analyses	Characteristics		C-alkylation (2)	O-alkylation (3)
¹ H	H _{6a} and H _{6b}	δ	AB part of ABXY system (2.22 & 2.64)	AB part of ABX system (4.48 & 4.58)
		Multiplicity	ddd ^a (see coupling constants on Figure 1)	dd ^b (² J _{6a-6b} =11.4; ³ J _{6a-5} =2.0; ³ J _{6b-5} =5.2)
	H _{2'}	δ	3.89	4.44
		Multiplicity	dd ^b (see coupling constants on Figure 1)	s ^c
	H _{4'} and H _{6'}		AB parts of two ABX ₃ systems (4.52 & 4.55; 4.53 – accidental isochrony of A and B)	AB parts of two ABX ₃ systems (4.39 & 4.45; 4.25 & 4.36)
		³ J _{H-F}	³ J _{H4'a-F5'} = ³ J _{H4'b-F5'} = ³ J _{H6'a-F7'} = ³ J _{H6'b-F7'} = 8.3	³ J _{H4'a-F5'} = 8.7; ³ J _{H4'b-F5'} = 8.6; ³ J _{H6'a-F7'} = 7.9; ³ J _{H6'b-F7'} = 7.8
¹³ C	C _{1'}	δ	167.15 ^d	163.51
	C _{2'}	δ	47.87	71.44
	C _{3'}	δ	166.88 ^d	167.78

^a : double doublet of doublets; ^b : double doublet; ^c : singlet; ^d : values may be interchanged

3.1. ^1H NMR spectrum

3.1.1. Signal multiplicities of H_6 and H_2' in C-alkylation vs O-alkylation products:

The two H_6 protons form an ABXY system with H_5 and H_2' in the C-alkylation product (Figure 1), while they couple only with H_5 in the O-alkylation product (ABX system, Figure 2).

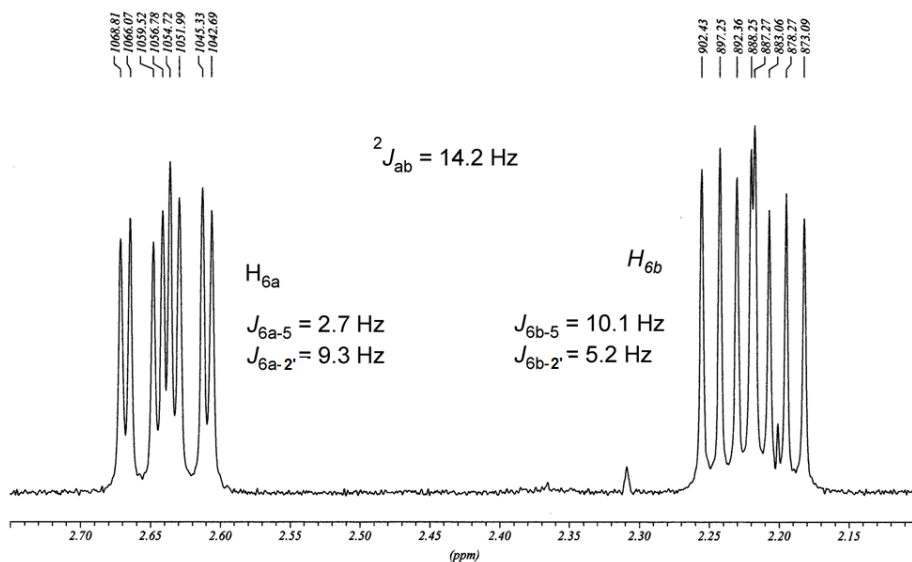


Figure 1. Signals of H_{6a} and H_{6b} for the C-alkylation product 2

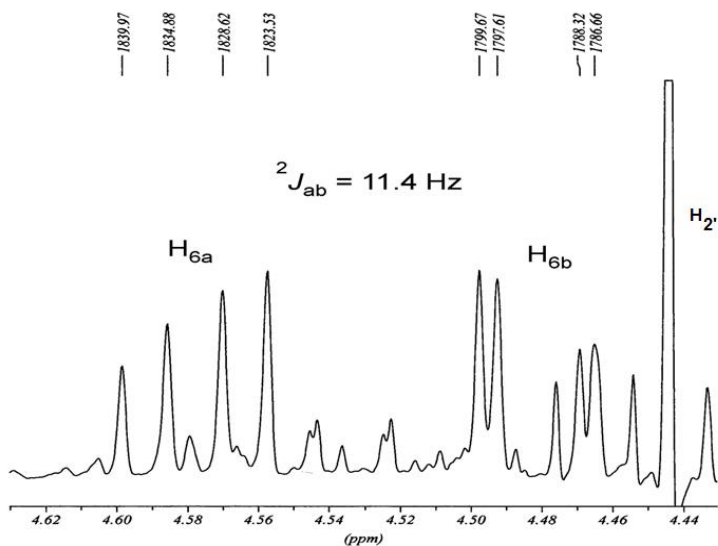


Figure 2. Signals of H_{6a} and H_{6b} for the O-alkylation product 3

$H_{2'}$ couples with the two H_6 protons (double doublet) in the C-alkylation product **2**, as seen in Figure 3, while its signal is a singlet in the O-alkylation product **3** (Figure 2).

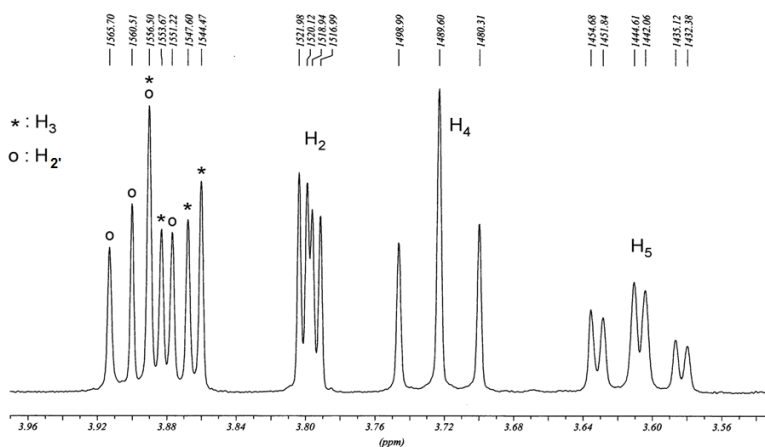


Figure 3. Signal of $H_{2'}$ for the C-alkylation product **2**

The coupling between the two H_6 and $H_{2'}$ is clearly observed in the 1H - 1H correlation spectrum (Figure 4).

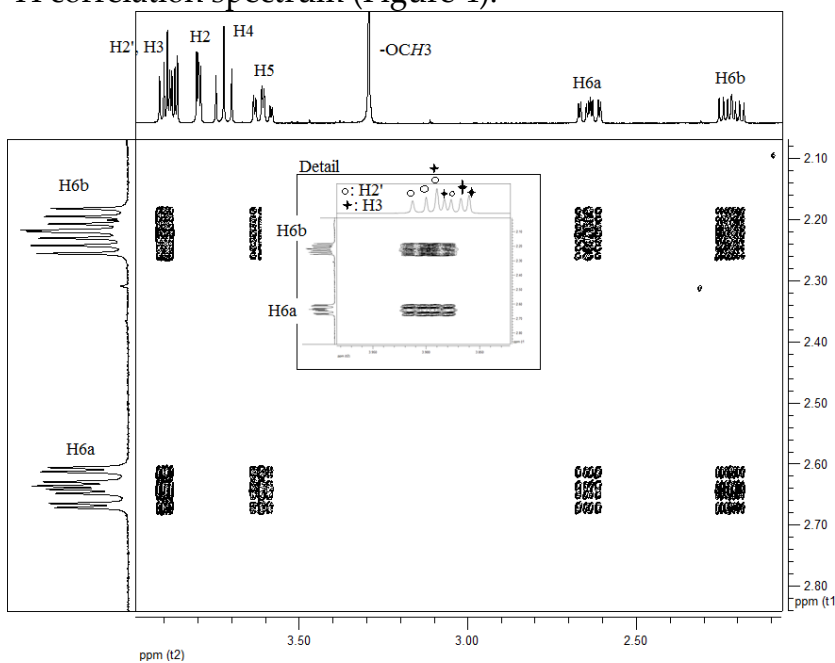


Figure 4. 1H - 1H NMR spectrum of the C-alkylated compound **2**. In the detail box, the spots corresponding to the coupling between H_{6a} and H_{6b} and $H_{2'}$ are outlined

Other differences regarding the ^1H NMR spectra of these two compounds may be noticed:

- Oxygen proximity has a deshielding effect over the H_6 protons in the *O*-alkylation product **3**, when compared to the *C*-alkylation product **2**.
- In product **3**, H_2' attached to a sp^2 carbon is strongly shielded due to the mesomeric effect of the two oxygen atoms on C_1' which creates a partial negative charge at C_2' . The same shielding is seen in the ^{13}C NMR spectra, when compared to classical alkenes chemical shifts [15].
- The coupling constant $^2J_{\text{H}_6\text{a}-\text{H}_6\text{b}}$ has a smaller value in the *O*-alkylation product **3** compared to that found in the *C*-alkylation product **2**. This observation is in agreement with literature data that states that the value of the geminal coupling constant in a methylene group decreases with the electronegativity of a neighboring heteroatom [16].

3.1.2. H_4' and H_6' in *C*-alkylation vs *O*-alkylation product:

Another interesting aspect is related to the signal of malonate residue protons (ABX_3 systems of CH_2CF_3 groups). In product **2**, the four $^3J_{\text{H-F}}$ coupling constants of the two $-\text{CH}_2\text{CF}_3$ groups have the same value 8.3 Hz, like that found in TFEM, an ester itself. In product **3**, the two groups have different coupling constants (two of them being smaller than 8 Hz and two larger) and therefore, a difference can be seen between $-\text{CH}_2\text{CF}_3$ groups linked to an ester and to an ether group. Moreover, these groups have different signal multiplicities (Table 1).

The example of the *C*-alkylation product will be given. In figure 5a, it can be seen that, although the two $-\text{CH}_2\text{CF}_3$ groups are symmetrical, one of the groups appears as an ABX_3 system, while the protons of the second $-\text{CH}_2\text{CF}_3$ group are isochronous at 400 MHz (appearing in the ^1H NMR spectrum as an A_2X_3 system). In figure 5b, it can be seen that, by irradiating the ^{19}F atoms, the ^1H - ^{19}F couplings disappear, and the signals of the first group become a simple AB system (indicated by rectangles, empty circles, full and empty stars), while the

signals of the second group become a singlet (indicated by full circles) (Figure 5b).

3.2. ^{13}C NMR spectrum

- C_2 : A clear difference can be seen in the ^{13}C NMR spectrum, as in the *O*-alkylation product, C_2' is more deshielded, shifting from around 50 ppm (compound 2, sp^3 carbon), to 70 ppm in compound 3 (sp^2 carbon). The shielding effect of oxygens next to the double bond has already been commented (section 3.1.1.).

- C_1' and C_3' : In the *C*-alkylation product, the malonate residue is symmetrical: both C_1' and C_3' are esters, and have similar chemical shifts (around 167 ppm, see Table 1). In the *O*-alkylation product, it can be noticed the fact that one ester group is present at 167.78 ppm, together with a carbon atom with a lower chemical shift (163.51 ppm, C_1'). This atypical high shift for a sp^2 $\text{C}=\text{C}$ carbon is due to the mesomeric effect of the two oxygen atoms on C_1' .

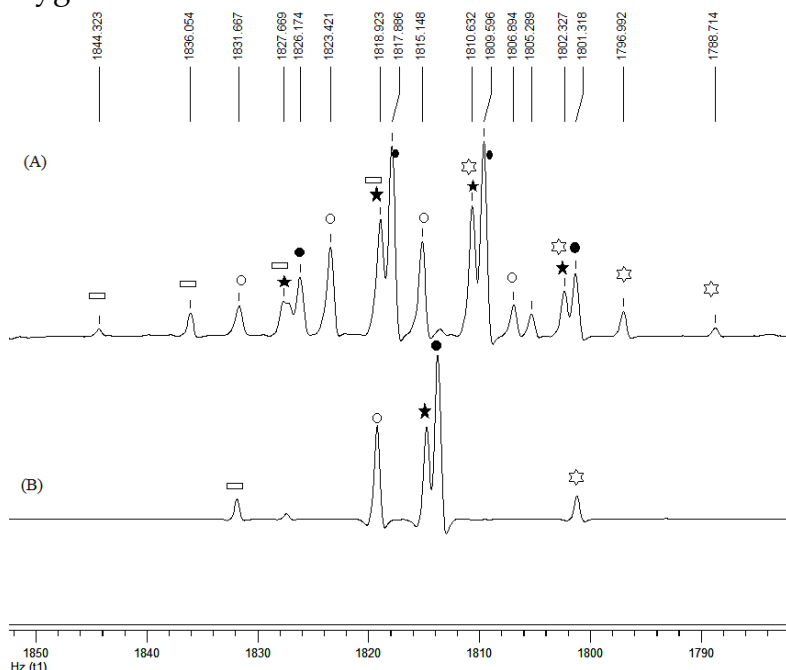


Figure 5. (A) Region of H_α and H_β in ^1H NMR spectrum of compound 2 (*C*-alkylation); (B) same spectrum as in (A) with ^{19}F irradiation – corresponding peaks in spectra (A) and (B) are indicated using specific signs (see text)

4. CONCLUSION

Each time ambident nucleophiles are used, there is a great interest in finding analyses tools able to distinguish between the possible reaction products. This work has applications in establishing the correct structure of other reaction products of TFEM or of C- or O-alkylated mannose derivatives. For example, the data presented in Table 1 were a great support in analysing the structure of the 6 compounds obtained when applying the Mitsunobu reaction with TFEM in the anomeric position of mannose, when only O-alkylation products have been obtained.

References

1. F. A. Carey, R. J. Sundberg, *Alkylation of Nucleophilic Carbon. Enolates and Enamines. In: Advanced Organic Chemistry*. Springer, Boston, MA (1990).
2. D. Seebach *Angew. Chem. Int. Ed.* 27 (1988) 1624.
3. C. Clavel, V. Barragan-Montero, J.-L. Montero, *Tetrahedron Lett.* 45 (2004) 7465.
4. C. Gurgui-Ionescu, L. Toupet, L. Uttaro, A. Fruchier, V. Barragan-Montero *Tetrahedron*, 63 (2007) 9345.
5. C. Ionescu, A. Fruchier, A. Moanta, M. Chelarescu, *Annals of the University of Craiova, The Chemistry Series*, XXXIX (2) (2010) 61.
6. O. Mitsunobu, M. Yamada, *Bull. Chem. Soc. Jpn.* 40 (1967) 2380.
7. For a review on Mitsunobu reaction, see: D. L. Hughes *Org. Prep. Proced. Int.*, 28 (1996) 127.
8. R. E. Hartung, M. C. Wall, S. Lebreton, M. Smrcina, M. Patek, *Heterocycles* 94 (2017) 1305.
9. D. L. Comins; G. Jianhua *Tetrahedron Lett.* 35 (1994) 2819.
10. J. Wang, C. D. Gutsche *Struct. Chem.* 12 (2001) 267.
11. M. Wada, O. Mitsunobu *Tetrahedron Lett.* 13 (1972) 1279.
12. T. K. M. Shing, L.-H. Li, K. J. Narkunan *Org. Chem.* 62 (1997) 1617.
13. N. G. Ramesh, K. K. Balasubramanian, *Tetrahedron* 51 (1995) 255.

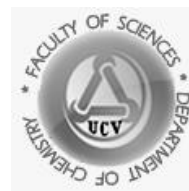
14. S. R. LaPlante, F. Bilodeau, N. Aubry, J. R. Gillard, J. O'Meara, R. Coulombe, *Bioorganic & Medicinal Chemistry Letters* 23 (2013) 4663.
15. E. Pretsch, P. Bühlmann, M. Badertscher, *Structure Determination of Organic Compounds* Springer-Verlag, Berlin Heidelberg, (2009).
16. H. Günther, *NMR Spectroscopy*, John Wiley & Sons, Chichester (1995).

Annals of the University of Craiova

The Chemistry Series

Volume XLIV, No. 2 (2017) 12-23

homepage: chimie.ucv.ro/anale/



Does the oxidation state impact chromium toxicity in wheat seedlings?

Research article

*Georgeta Ciobanu**, *Cătălina Ionescu*, *Aurora Reiss*

University of Craiova, Faculty of Sciences, Department of Chemistry, Calea Bucuresti, 107i, Craiova, Romania

*e-mail: geo_ciobanu20@yahoo.com

Received: 06.11.2017 / Accepted: 04.12.2017 / Published: 22.12.2017

Abstract

Dose-dependent growth inhibition was observed in wheat seedlings cultivated on media contaminated with chromium as CrCl_3 and $\text{K}_2\text{Cr}_2\text{O}_7$ respectively, ranging from $1 \mu\text{mol L}^{-1}$ to $500 \mu\text{mol L}^{-1}$. Biometric data pointed out $\text{Cr}_2\text{O}_7^{2-}$ as more effective than Cr^{3+} , with EC_{50} values of 0.15 mmol L^{-1} for root elongation inhibition and 0.23 mmol L^{-1} for stem elongation inhibition. At low levels of chromium excess, where growth inhibition didn't occur, modulation of some biochemical indexes (e.g. peroxidase activity, lipid peroxidation, glucose and anthocyanin content) was suggestive for the onset of adaptive responses of wheat plants.

Keywords: chromium, wheat plants, growth inhibition, biochemical effects

1. INTRODUCTION

Chromium (Cr), whose name of Greek origin is suggestive for the intense colour of its compounds, is a metallic element with the atomic number 24. Electronic configuration of elemental chromium is $[\text{Ar}]3d^54s^1$; accordingly, in the periodic table of elements it is placed in group 6 and period 4, among the transition metals. A wide range of oxidation states are possible for chromium, the most stable being +3 and +6. Chromium concentration in Earth's crust is about 100 ppm, the presence of its compounds in the environment being the result of rocks erosion and volcanic activity, with background concentrations, for example, lower than 500 mg kg^{-1} in soil and 0.5 mg kg^{-1} in vegetation [1].

Due to its properties, chromium has numerous practical uses. A 'short list' of these should contain: stainless steel obtaining and electroplating, dye and pigments, synthetic ruby and laser technology, wood preservation, leather tanning, refractory materials, and catalysts [2]. Thus, it is not surprising the extent of chromium environmental contamination due to anthropic activities, and the inherent risk that poses to ecosystems and human health [3]. Usually, Cr(III) is considered non-toxic, while Cr(VI) is known as toxic and carcinogenic. Hexavalent chromium is a powerful oxidant, and its reduction is safe when occurs outside cells, as the final product, Cr^{3+} , is less mobile, both in the environment and the living organisms. Biological reduction of Cr(VI) to Cr(III) is a potentially useful mechanism for Cr detoxification and bioremediation of the contaminated sites. In this respect, some bacterial activities are taken into account for environmental clean-up, and also for the purpose of chromium detoxification *in vivo* [4, 5].

Despite the efforts, chromium chemistry *in vivo* is still far from being clarified. The older idea about the essentiality of trivalent chromium in mammals, with a role in carbohydrate and lipid metabolism, was abandoned, as more recent findings do not support it [6, 7]. There are still gaps in understanding chromium genotoxicity and carcinogenicity [8-11]. In cells, the redox activity of hexavalent chromium lies at the heart of its toxicity. According to the current model emerging from literature on Cr(VI) genotoxicity, chromate anions enter the cell through the transporters of physiological anions (phosphate,

sulphate). When occurs within cells, besides depleting their antioxidants (ascorbate, glutathione), hexavalent chromium reduction generates reactive intermediates and oxidative stress. Moreover, once formed inside the cell, 'innocuous' Cr³⁺, the final product, may become very toxic by binding to macromolecules (nucleic acids, proteins) and preventing them from properly functioning [12].

Studies on chromium interactions with plants are also focused on topics like bioavailability, uptake, toxicity and detoxification [3, 13-15]. The present paper describes our findings on growth and certain biochemical parameters in wheat seedlings cultivated on media with excess chromium, ranging from 1 $\mu\text{mol L}^{-1}$ to 500 $\mu\text{mol L}^{-1}$, in two experimental series: one with chromium (III) as CrCl₃, and the other with Cr(VI), as K₂Cr₂O₇.

2. MATERIALS AND METHODS

2.1. Materials

All the solutions used in these experiments were prepared with analytical grade reagents. Wheat caryopses (*Triticum aestivum* L, cv. PB-1) were obtained from the Agricultural Research and Development Station Simnic, Dolj.

2.2. Plant cultivation and heavy metal treatment

Germinated wheat caryopses were cultivated on nutrient solutions solidified with agar [16, 17]. In order to evaluate the effects of chromium on wheat seedling growth, nutrient solutions were supplemented, in separated experiments, with CrCl₃ and K₂Cr₂O₇, respectively. For each of the abovementioned chromium salts, a series of dilutions ranging from 1 $\mu\text{mol L}^{-1}$ to 500 $\mu\text{mol L}^{-1}$ were obtained within the nutrient solutions, starting from 10 mmol L⁻¹ stock solutions. Each probe was ruled in triplicate, while 3 dishes without heavy metal excess were kept as control.

2.3. Plant growth assay

Seven days-old wheat plants were harvested and growth parameters (*i.e.* the length of the roots and stems) were registered. Biometric data were used for the calculation of growth inhibition index [17] and further to infer EC₅₀ values, the effective concentration that led to 50 % inhibition of wheat plants growth.

2.4. Biochemical assays

Few indexes of metabolic and redox status were assayed in wheat leaf extracts, prepared as we have previously described [17]. We aimed to find if any of the tested biochemical parameters were relevant for chromium toxicity, and to compare the effects of Cr(III) and Cr(VI), at concentration where no significant growth inhibition was observed. Total peroxidase activity (EC 1.11.1.7) was measured using guaiacol as reducing substrate [18], and the secondary lipid peroxidation products were dosed by TBARS assay [19]. The Bradford method was used for total soluble protein evaluation [20], while glucose content of the leaves was estimated by the glucose oxidase-peroxidase method [17]. Ethanolic extracts of leaf tissue were also prepared, and their absorption spectra in the visible domain were registered. The absorbance values at pigment-specific wavelengths were used to calculate chlorophylls and carotenoids concentration [21]. The pH differential method was used for anthocyanin content assay [22]. All the spectrophotometric measurements were carried out with a Varian Cary 50 UV-VIS spectrophotometer. Values of the abovementioned biochemical parameters were expressed in adequate units, and reported per fresh weight (*i.e.*, g⁻¹ FW). Data are averages of three measurements; standard deviations did not exceed 10 %.

3. RESULTS AND DISCUSSION

3.1. Biometric parameters of wheat plants

The observed inhibition of wheat seedling elongation at the highest tested concentration of Cr^{3+} ($500 \mu\text{mol L}^{-1}$) was about 25 % compared to control plants, both at root and stem level (Figure 1a). By contrast, a marked growth inhibition was noticed at the same concentration of $\text{Cr}_2\text{O}_7^{2-}$ in the growth medium, the respective wheat seedlings having up to 92 % shorter roots and 67 % shorter stems, compared to the unexposed plants (control; Figure 1b).

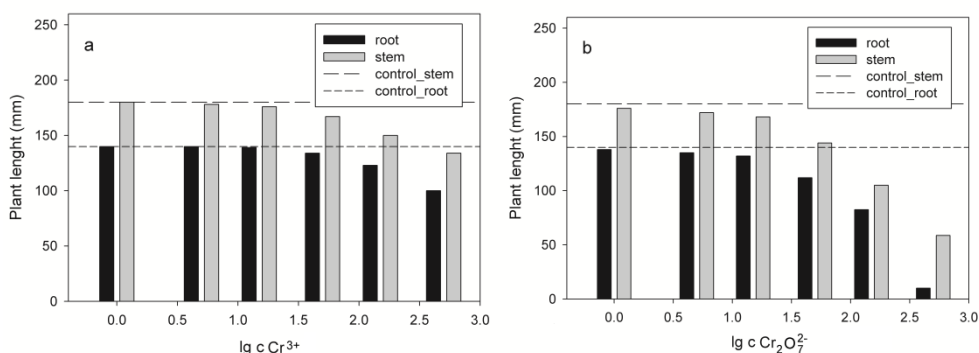


Figure 1. Growth parameters of wheat plants exposed to: a- Cr^{3+} b- $\text{Cr}_2\text{O}_7^{2-}$

Table 1. EC_{50} values for the inhibitory effect of Cr^{3+} and $\text{Cr}_2\text{O}_7^{2-}$ on wheat plants growth

	$EC_{50}/\text{mmol L}^{-1}$	
	root	stem
Cr^{3+}	1.22	1.39
$\text{Cr}_2\text{O}_7^{2-}$	0.15	0.23

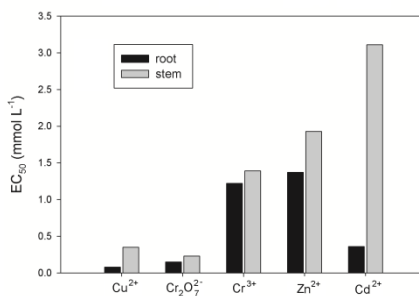


Figure 2. Comparison of the EC_{50} values of the tested metal ions for wheat growth inhibition

Shortly, the inhibitory effect of Cr^{3+} on wheat plant elongation was almost equal at root and stem level, while the oxyanion $\text{Cr}_2\text{O}_7^{2-}$ was more toxic on roots (Table 1). Compared with our previous results on Cu^{2+} , Cd^{2+} and Zn^{2+} toxicity [17], these data showed that Cr^{3+} was almost as toxic as Zn^{2+} while $\text{Cr}_2\text{O}_7^{2-}$ was less toxic than Cu^{2+} on roots but more toxic on shoots (figure 2). The observed effects are related to chromium speciation. Cr^{3+} binds tight to the anionic components of plant cell wall, its mobility and bioavailability being low. Supposed to entry cells by diffusion or endocytosis, chromium (III) cations are rather restrained outside the cell because of the selective permeability of plasma membrane. As a result of its low bioavailability, trivalent chromium exhibits low toxicity. By contrast, chromium (VI) oxyanions are not trapped at cell wall level, are more mobile in plant and can cross the plasma membrane through transport proteins. Greater mobility compared to Cr^{3+} explains for the observed greater toxicity of $\text{Cr}_2\text{O}_7^{2-}$ both at root and stem level.

3.2. Antioxidant and metabolic indexes of wheat plants exposed to heavy metals

In the leaves of wheat plants unexposed to heavy metals, *peroxidase activity* was of $2.41 \text{ U g}^{-1} \text{ FW}$. Enzyme's activity doubled when plants grew on media with 1 and $5 \mu\text{mol L}^{-1} \text{ Cr}_2\text{O}_7^{2-}$ as well as at $1 \mu\text{mol L}^{-1} \text{ Cr}^{3+}$, and a 1.6 times increase was observed at $5 \mu\text{mol L}^{-1} \text{ Cr}^{3+}$. Peroxidase responses were almost similar, irrespective the oxidation state or tested concentrations of exogenous chromium (Figure 3a). The observed boost of antioxidant defence may suggest an increased generation of hydrogen peroxide. Marked increase of peroxidase activity were previously reported in the leaves of wheat plants exposed to excess copper and cadmium [17, 23], and appears as a first line of defence in plants intoxicated with heavy metals.

Lipid peroxidation. The leaves of wheat plants grown in the absence of heavy metal contamination had a concentration of secondary lipid peroxidation products (TBARS- thiobarbituric acid reactive substances) of approximately $100 \mu\text{mol g}^{-1} \text{ FW}$. Increased lipid peroxidation was noticed in chromium exposed plants, compared to control: with 10 % in Cr^{3+} probes and 45 % in $\text{Cr}_2\text{O}_7^{2-}$ probes, at both 1

and $5 \mu\text{mol L}^{-1}$ (Figure 3b). These data suggested that $\text{Cr}_2\text{O}_7^{2-}$ exposure is associated with advanced lipid peroxidation that could occur because of the redox activity of chromium *in vivo*. Among the metals whose phytotoxic effects were assayed within our studies, chromium, as $\text{Cr}_2\text{O}_7^{2-}$, appeared as the main promoter of lipid peroxidation.

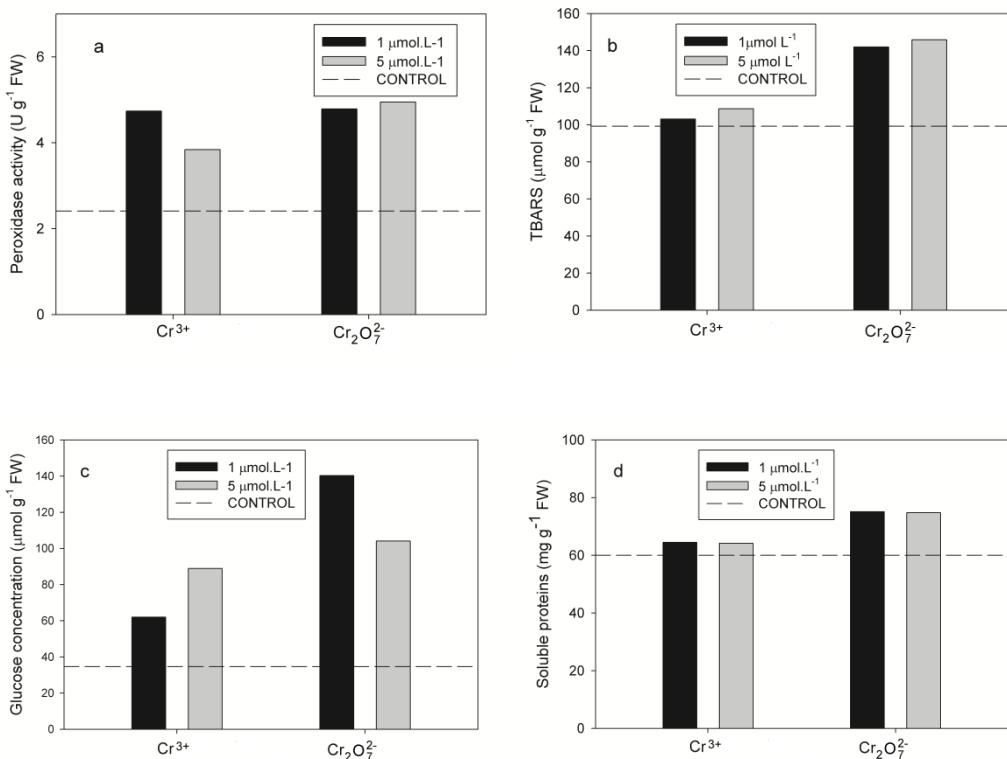


Figure 3. Biochemical parameters of wheat plants exposed to Cr^{3+} and $\text{Cr}_2\text{O}_7^{2-}$: a – peroxidase activity, b – secondary lipid peroxidation products (TBARS) c – glucose, and d – soluble proteins

Glucose concentration in the leaves of unstressed wheat plants was of $34.69 \mu\text{mol g}^{-1} \text{FW}$. Dose dependent increases of glucose concentration were observed in Cr^{3+} probes, with 1.8 and 2.5 times respectively at the two tested concentrations. Increased glucose concentration were also noticed in $\text{Cr}_2\text{O}_7^{2-}$ exposed wheat seedlings, with 4 and respectively 3 times greater than leaf glucose content in control plants (Figure 3c).

Thus, glucose concentration appeared as the most susceptible parameter when excess chromium was present in plant's growth media. Our previous data on heavy metal exposed wheat seedlings also noticed increased glucose levels in copper and cadmium probes, but to a less extent than in chromium ones [17].

Under the given experimental condition, the amount of *total soluble proteins* in the leaves of wheat plants unexposed to chromium salts was of 60 mg g⁻¹ FW. Compared to control plants, protein content in wheat seedlings grown on media with excess Cr³⁺ was less than 10 % greater. In case of Cr₂O₇²⁻ exposure, 25 % increases of the same parameter were observed at both tested concentrations (Figure 3d). Thus, variations of the soluble proteins content appeared to depend more on exogenous chromium speciation than on its concentration. Metal speciation *in vivo* is a complex and difficult to evaluate issue that may have an essential impact on its effects. Our previous results on wheat seedlings exposed to similar doses of Cu²⁺, Cd²⁺ and Zn²⁺ revealed minor increases of soluble protein content in the leaves [17]. These results are consistent with the importance of proteins as fundamental, structural and functional constituents of the living tissues.

3.2. Leaf pigments in wheat plants exposed to heavy metals

Concentrations of the photosynthetic pigments in control wheat plants were as it follows: 1.52 μmol g⁻¹ FW *total chlorophylls* (comprising 1.12 μmol g⁻¹ FW Chl *a* and 0.4 μmol g⁻¹ Chl *b*) and 0.40 μmol g⁻¹ *total carotenoids*. Leaf pigments concentration in plants grown on media contaminated with chromium salts decreased in certain experimental probes compared to control (Figure 4, a-c). *Chlorophyll a* content was 20 % lower than control at both 1 and 5 μmol L⁻¹ Cr³⁺, as well as at 1 μmol L⁻¹ Cr₂O₇²⁻; no difference from control was observed at 5 μmol L⁻¹ Cr₂O₇²⁻. *Chlorophyll b* concentrations decreased with 15 % at both 1 and 5 μmol L⁻¹ Cr³⁺; a 25 % decrease was observed at 1 μmol L⁻¹ Cr₂O₇²⁻, while no variation compared to control was noticed at 5 μmol L⁻¹ Cr₂O₇²⁻. *Carotenoids* content decreased with 15 % compared to control at the lowest chromium concentrations tested, irrespective the metal

speciation; less than 10 % decrease was observed at 5 $\mu\text{mol L}^{-1}$ Cr^{3+} , and no difference at 5 $\mu\text{mol L}^{-1}$ $\text{Cr}_2\text{O}_7^{2-}$.

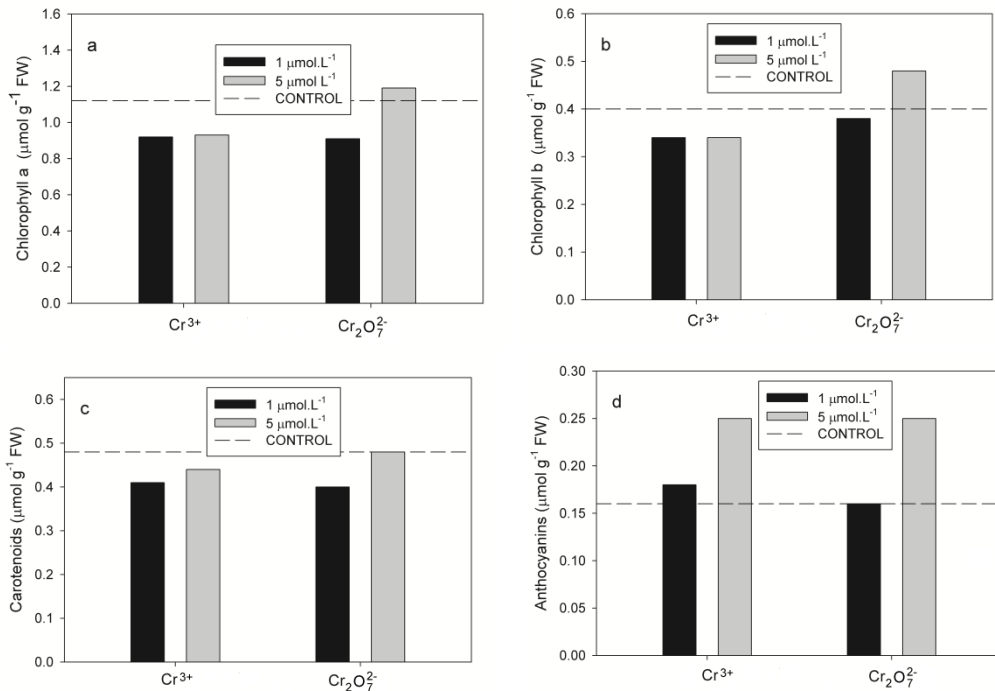


Figure 4. Leaf pigments in wheat plants exposed to Cr^{3+} and $\text{Cr}_2\text{O}_7^{2-}$: a – chlorophyll *a*, b – chlorophyll *b*, c – carotenoids, and d – anthocyanins

The calculated values of *Chl a:Chl b* ratio for the heavy metal exposed plants within our experiments, as well as those of *Car:Chl* ratio, were quite similar to the ones of control plants (Table 2). Taking into account both these data and those we've previously presented referring to Cu, Zn and Cd effects [17], one can conclude that although lower quantities of photosynthetic pigments were dosed in the leaves of certain heavy metal exposed wheat plants compared to control plants, values of the abovementioned indexes didn't significantly vary compared to control. *Chl a:Chl b* and *Car:Chl* ratios are often used to assess whether photosystem I or photosystem II are affected or not by different stresses to which plants are exposed [24]. According to this assumption, we can conclude that the experimental conditions in our study didn't significantly affect the photosystems. Modulation of the

pigments' content served the purpose of adaptation and efficient use of the light absorbed by the photosystems.

Leaf *anthocyanins* concentration in untreated wheat plants was of 0.16 $\mu\text{mol g}^{-1}$ FW. Compared to control plants, anthocyanin content in the leaves of chromium exposed plants registered no increase or low increase at 1 $\mu\text{mol L}^{-1}$ Cr^{3+} and $\text{Cr}_2\text{O}_7^{2-}$, respectively. By contrast, about 50 % greater anthocyanin concentrations than in control plants were dosed in leaves of the wheat plants exposed to 5 $\mu\text{mol L}^{-1}$ of both tested chromium salts (Figure 4, d).

Table 2. Chl *a*: Chl *b* and Car: Chl ratios for wheat plants exposed to Cr^{3+} and $\text{Cr}_2\text{O}_7^{2-}$

<i>Cr salt</i> $\mu\text{mol L}^{-1}$	<i>Chl a: Chl b</i>			<i>Car: Chl</i>		
	control	Cr(III)	Cr(VI)	control	Cr(III)	Cr(VI)
1	2.8	2.71	3.03	0.32	0.33	0.33
5	2.8	2.66	2.92	0.32	0.34	0.32

Comparing these data with those presented in the first part of our study, 50 % or more increased anthocyanin content *vs.* control was observed at 5 $\mu\text{mol L}^{-1}$ of the tested heavy metals within the growth media, while no significant differences were noticed at 1 $\mu\text{mol L}^{-1}$ [17]. Thus, it appears that increased anthocyanin content was mostly related to concentration than to speciation of chromium, being otherwise a non-specific response to heavy metal excess. Among the tested metals within this study, cadmium resulted as the most efficient inductor of anthocyanin accumulation in the leaves of young wheat plants.

4. CONCLUSIONS

Growth inhibition of wheat seedlings was the net outcome of their exposure for 7 days to chromium salts, at concentrations up 500 $\mu\text{mol L}^{-1}$ in their growth media. EC_{50} values for the observed inhibitory effect pointed out that $\text{Cr}_2\text{O}_7^{2-}$ was more effective than Cr^{3+} in this regard. Biochemical indexes of wheat seedlings, at chromium

concentrations where no growth inhibition was observed, are suggestive for the onset of defense responses. Among these, the most prominent were: increased peroxidase, to cope excess hydrogen peroxide, increased glucose concentration for cellular respiration, osmoregulation and signalling, and increased anthocyanins content, for free radical scavenging and photoprotection.

References

1. J. Emsley, *Nature's Building Blocks: An A-Z Guide to the Elements*, Oxford University Press, London (2001).
2. N. T. Joutey, H. Sayel, W. Bahafid, N. El Ghachtouli, *Rev. Environ. Contam. Toxicol.*, 233 (2015) 46.
3. H. Oliveira, *J. Bot.*, (2012) doi:10.1155/2012/375843.
4. C. VitiC. V, E. Marchi, F. Decorosi, L. Giovannetti, *FEMS Microbiol. Rev.*, 38 (2014) 633.
5. S. Younan, G. Z. Sakita, T.R. Albuquerque, R. Keller, H. Bremer-Neto, *J. Sci. Food Agric.*, 96 (2016) 3977.
6. K. R. Di Bona, S. Love, N. R. Rhodes, et al., *J. Biol. Inorg. Chem.*, 16 (2011) 381.
7. J. B. Vincent, *Met. Ions Life Sci.*, 13 (2013) 171.
8. S. S. Wise, J. P. Wise, Sr., *Mutat. Res.*, 733 (2012) 78.
9. K. P. Nickens, S. R. Patierno, S. Ceryak, *Chem. Biol. Interact.*, 188 (2010) 276.
10. A. Zhitkovich, *Chem. Res. Toxicol.*, 24 (2011) 1617.
11. Y. Wang, H. Su H, Y. Gu, X. Song, J. Zhao, *Onco Targets Ther.*, 10 (2017) 4065.
12. C. M. Thompson, L. C. Haws, M. A. Harris, N. M. Gatto, D. M. Proctor, *Toxicol. Sci.*, 119 (2011) 20.
13. H. P. Singh, P. Mahajan, S. Kaur, D. R. Batish, R. K. Kohli, *Environ. Chem. Lett.*, 11 (2013) 229.
14. M. A. da Conceição Gomes, R. A. Hauser-Davis, M. S. Suzuki, A. P. Vitória, *Ecotoxicol. Environ. Saf.*, 140 (2017) 55.
15. M. Shahid, S. Shamshad, M. Rafiq, S. Khalid, I. Bibi, N. K. Niazi, C. Dumat, M. I. Rashid, *Chemosphere*, 178 (2017) 513.
16. V. Page, U. Feller, *Ann. Bot-London*, 96 (2005) 425.

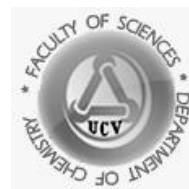
17. G. Ciobanu, C. Ionescu, M. Mateescu, *Annals of the University of Craiova, The Chemistry Series*, Volume XLIV, No 1, **(2017)** 36.
18. H. U. Bergmeyer, *Methods of Enzymatic Analysis 1*, Academic Press, New York **(1974)**.
19. H. H. Draper, M Hadley, *Methods Enzymol.*, 186 **(1990)** 421.
20. M. M. Bradford, *Anal. Biochem.*, 72 **(1976)** 248.
21. K. Lichtenthaler, *Methods Enzymol.*, 148 **(1987)** 350.
22. R. E. Wrolstad, R. W. Durst, J. Lee, *Trends Food Sci. Tech.*, 16 **(2005)** 423.
23. G.Matei, C. Babeanu, M. Soare, O. F.Birzanu, *Annals of the University of Craiova-Agriculture, Montanology, Cadastre Series*, 43 **(2013)** 211.
24. R. Tanaka, A. Tanaka, *Biochim. Biophys Acta*, 1807 **(2011)** 968.

Annals of the University of Craiova

The Chemistry Series

Volume XLIV, No. 2 (2017) 24-35

homepage: chimie.ucv.ro/anale/



Azoethers and azoesters with antimicrobial activity

An overview

*Anca Moanță**, *Cătălina Ionescu*, *Simona Iordache*

University of Craiova, Faculty of Sciences, Department of Chemistry, Calea Bucuresti, 107i, Craiova, Romania

*E-mail: moantaanca@yahoo.com

Received: 20.10.2017 / *Accepted:* 28.11.2017 / *Published:* 22.12.2017

Abstract

Infectious diseases are caused by the presence of bacteria and fungi in living organisms. Many drugs are used to combat them: sulfonamides, tetracyclines, quinolones, polypeptides, penicillins, cephalosporins, cabapenems, aminoglycosides. In recent years, many azoderivatives have been studied and have been shown to exhibit antimicrobial activity. This paper provides a review regarding the azomonoethers and the azoethers with antibacterial or antifungal activity.

Keywords: azoderivatives, 4-(phenylazo)phenoxyacetic acids, azoethers, azoesters, antimicrobial activity

1. INTRODUCTION

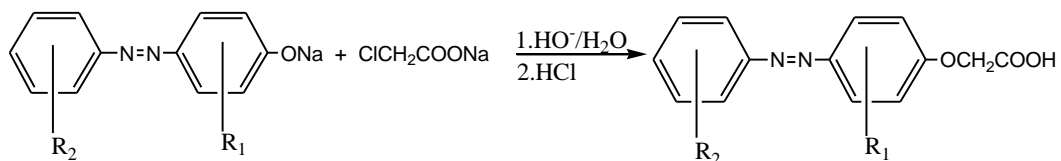
Azoderivatives are organic compounds possessing an azo group. They have the general formula $R-N=N-R$, where R is an aryl radical. They have possible applications in fibres dyeing, biochemistry, biology, medicine, analytical chemistry, but also as alimentary additives, chromophores in non-linear optics and in the inhibition of carbon-steel corrosion [1,2].

In recent years, many studies have been devoted to the synthesis of azoderivatives possessing different types of bioactivities: antibacterial [3,4], antifungal [5], anti-inflammatory [6,7] and antiviral activities [8]. Congo red exhibits ameliorative effects in models of neurodegenerative disorders: Alzheimer's, Parkinson's, Huntington's and prion diseases [9].

In this review, four types of azoderivatives that have antimicrobial activity: 4-(phenylazo)phenoxyacetic acids [10-12], 4-phenyldiazenyl-4'-[(4-chlorobenzyl)oxy]biphenyls [13], 4-[(4-chlorobenzyl)oxy]azobenzenes [14,15] and 4-(phenyldiazenyl)phenyl benzenesulfonate [16] are presented.

1. 4-Phenylazophenoxyacetic acids

The 4-(phenylazo)phenoxyacetic acids contain an azo group, a carboxyl group and two aromatic rings, substituted with various substituents: chloro, bromo, methyl or allyl. They were prepared by the condensation of sodium salts of corresponding substituted 4-phenylazophenols with chloroacetic acid in alkaline medium, using Williamson method (Scheme 1).



Scheme 1. Synthesis of the 4-(phenylazo)phenoxyacetic acids

Table1. Antimicrobial activities of 4-(phenylazo)phenoxyacetic acids

No.	Compound	Diameter of zone of inhibition in mm				
		S. <i>aureus</i>	S. <i>pyogenes</i>	E. <i>coli</i>	P. <i>aeruginosa</i>	P. <i>vulgaris</i>
1	2-methyl-4-phenylazo-phenoxyacetic acid	15	7	18	15	20
2	3-methyl-4-phenylazo-phenoxyacetic acid	16	18	7	13	15
3	4-(2-methyl-phenylazo)-phenoxyacetic acid	18	20	21	10	20
4	2,3-dimethyl-4-phenylazo-phenoxyacetic acid	8	10	12	15	8
5	2,6-dimethyl-4-phenylazo-phenoxyacetic acid	8	7	9	20	20
6	2-methyl-4-(4-methyl-phenylazo)-phenoxyacetic acid	9	10	7	10	12
7	4-(4-chloro-phenylazo)-phenoxyacetic acid	18	-	9	20	-
8	2,5-dichloro-4-(4-chloro-phenylazo)-phenoxyacetic acid	22	20	-	-	-
9	2-chloro-4-phenylazo-phenoxyacetic acid	12	-	7	15	-
10	2-bromo-4-phenylazo-phenoxyacetic acid	16	-	-	-	-
11	2-allyl-4-(4-chloro-4-phenylazo)-phenoxyacetic acid	18	-	-	-	-

These acids are colored powders. The color of compounds is also confirmed by the UV-Vis spectra containing a low intensity R-band at 430-452 nm, due to the -N=N- chromophore. A middle intensity B-band at 220-248 nm, consequently to the π electrons conjugation from the aromatic rings and an intense absorption K-band at 344-362 nm, as the result of the conjugated system Ar-N=N-Ar were also observed. Other evidence to confirm the structure was obtained from the IR, ¹H-NMR and mass spectra. IR spectra show absorption bands specific to -COOH (3473-3453 cm⁻¹ and 1740-1680 cm⁻¹), -N=N- (1600-1550 cm⁻¹ and 1430-1400 cm⁻¹), Ar-O-CH₂ (1276-1200 cm⁻¹ and 1078-1000 cm⁻¹), and to the aromatic rings (1600-1450 cm⁻¹). The fragmentation observed in mass spectra is achieved by the cleavage of the bond between the C of the methylene group and C atoms of the carboxyl, the C-N bonds and the O-CH₂ bond. Three common signals appear in the ¹H NMR spectra of all

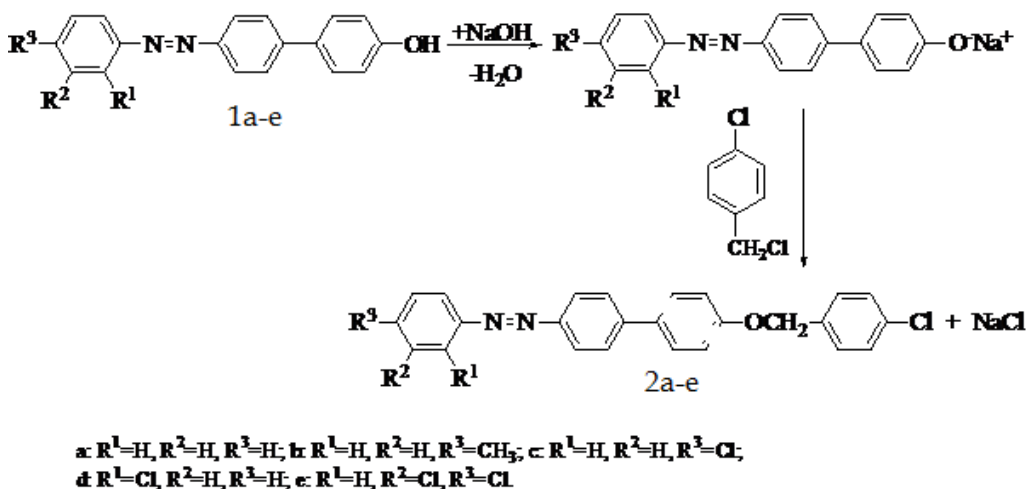
compounds: a singlet at $\delta=4.5-5.5$ ppm (CH_2 group), a singlet at $\delta=10.1-11.1$ ppm (COOH protons), a multiplet at $\delta=6.9-8.7$ ppm (the aromatic protons).

The 4-phenyldiazenyl-phenoxyacetic acids thus described were subjected to antimicrobial activity screening against two gram-positive bacteria (*S. aureus* and *S. pyogenes*), three gram-negative bacteria (*P. aeruginosa*, *P. vulgaris* and *E. coli*) and one fungi species (*C. albicans*) employing the disk diffusion technique (Table 1).

The best efficiency was exhibited by all compounds having a methyl substituent. All tested compounds tested are inactive against *C. albicans* species.

2. 4-phenyldiazenyl-4'--[(4-chlorobenzyl)oxy]biphenyls

4-phenyldiazenyl-4'--[(4-chlorobenzyl)oxy]biphenyls are derivatives of biphenyl having two radicals in para positions: phenylazo and (4-chlorobenzyl)oxy. They can be substituted by chlorine and methyl groups. They are azomonoethers prepared using the etherification of the corresponding sodium salts of substituted 4'-phenyldiazenyl-biphenyl-4-ols with 1-chloro-4-(chloromethyl)benzene in alkaline medium (Scheme 2) employing the Williamson method.



Scheme 2. Synthesis of the 4-phenyldiazenyl-4'--[(4-chlorobenzyl)oxy] biphenyls

The structure of these compounds has been investigated on the basis of UV-visible, IR, ^1H NMR and mass spectra.

The electronic spectra, recorded in dioxan, exhibit a R-band due to azo-group at 432-452 nm, a high intensity K-band due to the conjugated system Ar-N=N-Ar at 338-344 nm and a high intensity B-band due to the aromatic rings at 234-263 nm.

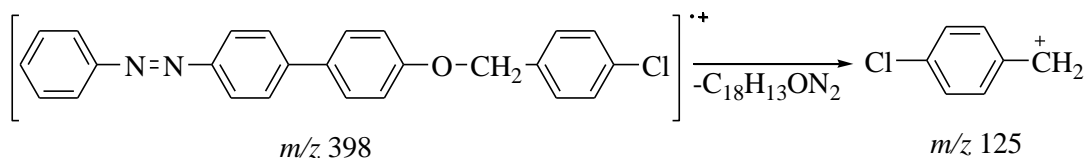
The infrared spectra confirm the presence of azo and ether groups in the structure of the obtained compounds. The vibration frequency of the N=N group appears at 1400-1413 cm^{-1} . The proofs of the etherification reaction between the hydroxyl group of azophenol and the 1-chloro-4-(chloromethyl)benzene are:

-the absence in the IR spectra of the bands characteristic for the hydroxyl group;

-the presence of absorption bands of the C-O-C newly formed group; thus spectrum contains an intensive absorption band at 1260-1280 cm^{-1} which can be assigned to the antisymmetrical valence vibrations of the C-O-C group and a moderate absorption band due to the symmetrical valence vibrations of the C-O-C group at 1013-1014 cm^{-1} .

The ^1H NMR spectra of all compounds show that the signal of the CH_2 group appears like a singlet at values between $\delta = 5.0 - 5.5$ ppm. The aromatic protons from the four substituted benzene rings came into resonance as a multiplet at $\delta = 7.2 - 7.7$ ppm. For 4-(4-methylphenyldiazenyl)-4'-[(4-chlorobenzyl)oxy]biphenyl an additional singlet is present at $\delta = 2.2$ ppm, corresponding to the methyl group protons.

The fragmentation pattern described in Scheme 3 for 4-phenyldiazenyl-4'-[(4-chlorobenzyl)oxy]biphenyl, is characteristic for all compounds:



Scheme 3. Fragmentation of 4-phenyldiazenyl-4'-[(4-chlorobenzyl)oxy]biphenyl under electron impact ionization

Scheme 3 shows a major fragmentation of 4-phenyldiazenyl-4'-[(4-chlorobenzyl)oxy]biphenyl in which the molecular ion peak at m/z 398 is abundant and the molecule tends to undergo a cleavage of the O-CH₂ bond to give the base peak at m/z 125.

The antibacterial activity of the investigated 4-phenyldiazenyl-4'-[(4-chlorobenzyl)oxy]biphenyls was done by microdiscs paper diffusion against three gram-positive bacteria (*S. aureus*, *S. pyogenes*, *B. subtilis*) and four gram-negative bacteria (*K. pneumonia*, *S. paratyphae*, *P. vulgaris* and *E. coli*). Chloramphenicol was used as standard drug.

Table 2. Antimicrobial activities of the 4-phenyldiazenyl-4'-[(4-chlorobenzyl)oxy] biphenyls

No.	Name of compound	Diameter of zone of inhibition in mm / Relative percentage of inhibition in %				
		<i>S. paratyphae</i>	<i>E. coli</i>	<i>B. subtilise</i>	<i>K. pneumonia</i>	<i>P. vulgaris</i>
1	4-phenyldiazenyl-4'-[(4-chlorobenzyl)oxy]biphenyl	21.66/ 81.45	21.33/ 50.55	23.33/ 54.43	10/ 12.75	24.66/ 97.29
2	4-(4-methyl-phenyldiazenyl)-4'-[(4-chlorobenzyl)oxy]biphenyl	20/ 69.44	24.66/ 67.56	26/ 75.11	11.33/ 16.37	22.33/ 72.79
3	4-(4-chloro-phenyldiazenyl)-4'-[(4-chlorobenzyl)oxy]biphenyl	22.33/ 86.56	28/ 87.11	24.33/ 65.77	12/ 18.36	18/ 51.84
4	4-(2-chloro-phenyldiazenyl)-4'-[(4-chlorobenzyl)oxy]biphenyl	18.66/ 60.45	30/ 100	11.66/ 85	11.66/ 17.34	16.66/ 44.40
5	4-(3,4-dichloro-phenyldiazenyl)-4'-[(4-chlorobenzyl)oxy]biphenyl	19.33/ 64.87	25.33/ 71.29	12.66/ 83	12.66/ 20.44	17/ 46.24
6	Chloramphenicol	24	30	30	28	25

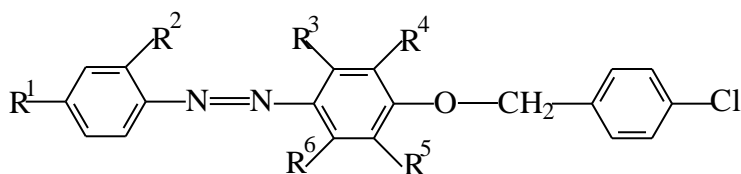
Results revealed that in general, all tested compounds possessed good antibacterial activity against three gram-negative bacteria (*S. paratyphae*, *P. vulgaris* and *E. coli*). The best efficiency at the tested concentrations was exhibited by 4-(2-chloro-phenyldiazenyl)-4'-[(4-chlorobenzyl)oxy]biphenyl against *E. Coli* and by 4-phenyldiazenyl-4'-[(4-chlorobenzyl)oxy]biphenyl against *P. vulgaris* (Table 2). The compounds exhibited moderate activity against *K. pneumonia*. Interpretation of antibacterial screening data revealed that all the tested

compound showed good inhibition on the growth of *B. subtilis* (Table 2). All tested 4-phenyldiazenyl-4'-[(4-chlorobenzyl)oxy]biphenyls are inactive against *S. pyogenes* and *S. aureus*.

The results of antibacterial activity of the tested compounds were compared with the standard drug for evaluating their relative percentages of inhibition (Table 2). The maximum relative percentage of inhibition was exhibited by 4-(2-chloro-phenyldiazenyl)-4'-[(4-chlorobenzyl)oxy]biphenyl against *E. coli* (100 %), followed by 4-phenyldiazenyl-4'-[(4-chlorobenzyl)oxy] biphenyls against *P. vulgaris* (97.29 %).

3. 4-[(4-chlorobenzyl)oxy]azobenzenes

4-[(4-Chlorobenzyl)oxy]azobenzenes are azomonoethers having the general formula:



$R^1=H, Cl, CH_3$; $R^2=H, Cl$; $R^3=H, CH_3$; $R^4=H, Cl, CH_3$; $R^5=H, CH_3$; $R^6=H, Cl, CH_3$;

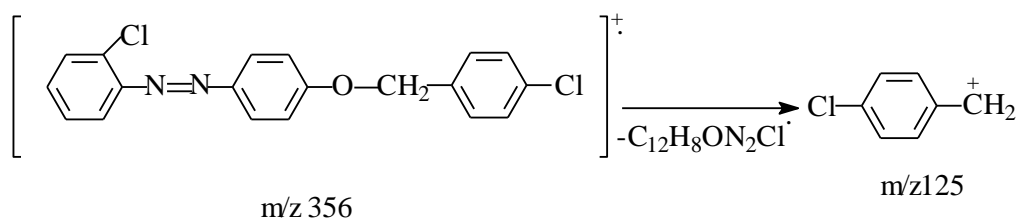
Scheme 4. Structure of 4-[(4-chlorobenzyl)oxy]azobenzenes

Ten azomonoethers were prepared by condensation of 4-chloromethyl-chlorobenzene with various azophenols substituted by chlorine and methyl groups. The Williamson method for the preparation of ethers was used. This method has also been used to synthesize azomonoethers, azobisethers, bisazobisethers and poliazoarylenethers [1].

Their structure was assumed from the chemical reaction equation. It was confirmed using spectral methods. In UV-Vis spectra, various bands were observed: E bands at 235-247 nm ($\pi \rightarrow \pi^*$ transitions), B bands at 247-250 nm (aromatic rings), K bands at 345-370 nm (conjugate system Ar-N=N-Ar) and R bands at 435-440 nm (azo group). IR spectra show absorption bands characteristic of the group of

atoms in the molecule: C-H from CH₃ groups at 2918-2906 cm⁻¹, azo group at 1430-1400 cm⁻¹ and 1603-1567 cm⁻¹, C-O-C group at 1200-1300 cm⁻¹ and C-Cl at 818-812 cm⁻¹. NMR ¹H spectra contain two signals: one multiplet at 6.1-7 ppm (aromatic protons) and un singlet at 3.6-4.3 ppm. Azomonoethers containing a methyl group present also have a singlet at 1.1-1.8 ppm (-CH₂-). Mass spectra provide additional evidence for the structure of these azomonoethers. They were used to determine the molecular weight.

The fragmentation pattern described in Scheme 5 for 4-[(4-chlorobenzil)oxi]-2'-cloro-azobenzen, is characteristic for all azomonoethers:



Scheme 5. Fragmentation of 4-[(4-chlorobenzil)oxi]-2'-cloro-azobenzen under electron impact ionization

The O-CH₂ bond is breaks and a base peak is formed at m/z 125 for all compounds.

Antimicrobial activity of azomonoethers was tested against *S. aureus*, *S. pyogenes*, *P. aeruginosa*, *P. vulgaris*, *E. coli* and *C. albicans* using the disk diffusion method. All bacteria are resistant to the presence of test compounds. The growth of *C. albicans* is inhibited by four isomers. Thus, the diameter of the inhibition zone is 20 mm, 15 mm, 12 mm and 18 mm for 4-[(4-chlorobenzyl)oxy]-2-methyl-4'-chloro-azobenzene, 4-[(4-chlorobenzyl)oxy]-3-chloro-4'-methyl-azobenzene, 4-[(4-chlorobenzyl)oxy]-3-methyl-4'-chloro-azobenzene and 4-[(4-chlorobenzyl)oxy]-2-methyl-2'-chloro-azobenzene, respectively.

4.4-(phenyldiazenyl)phenyl benzenesulfonate

4-(Phenyldiazenyl)phenyl benzenesulfonate (PPB) is an azoester containing SO₂ group and azo group. PPB was synthesized because:

a) It is known that there are a lot of compounds carrying SO₂ groups and having antimicrobial activity against *S. aureus*, *E. coli*, *C. albicans* and *C. parapsilosis* [17-18].

b) A great number of azoderivatives are reported to show an antimicrobial activity: 2-[(E)-2-(3-acetyl-4-hydroxyphenyl)-1-diazenyl]benzoic acid [19], 4-phenylazo-phenoxyacetic acids having chloro or methyl substituents [10], 4-[(4-chlorobenzyl)oxy]azobenzenes [14] and 4-phenyldiazenyl-4'-[(4-chlorobenzyl)oxy]biphenyls [13].

PPB was obtained by a coupling reaction between 4-(phenyldiazenyl)phenol and benzenesulfonyl chloride in the presence of pyridine [20]. The structure of the azo-ester is shown in Scheme 6.



Scheme 6. Structure of PPB

The structure of the compound was demonstrated using:

-UV-Vis spectra in dioxane ($\lambda_{\text{max}}=321$ nm, $\lambda_{\text{max}}=441$ nm for azo group);

-FTIR spectra (C₆H₅-N=N-, -C-C-, -C=C-, C₆H₅-SO₂-, C₆H₅-SO₃-, C₆H₅-O-, C₆H₅-);

-¹H NMR (aromatic protons between 7.13 ppm and 7.91 ppm).

-mass spectra under electron impact (base peak at m/z 77, molecular peak at m/z 338).

PPB was screened for its antimicrobial activity against two gram-positive bacteria (*S. aureus* and *S. pyogenes*), three gram-negative bacteria (*P. aeruginosa*, *P. vulgaris* and *E. coli*), and two fungi species (*C. albicans* and *A. niger*). The antimicrobial inhibition zones (mm) were determined using the disk diffusion method. Cloramfenicol was used as standard drug (Figure 1) and methanol served as control.

Table 3. Antimicrobial activity of PPB

Name of organisms	Mean zone of inhibition \pm Standard deviation (mm)			Relative percentage inhibition (%)
	PPB	Cloramfenicol	Methanol	
<i>Staphylococcus aureus</i>	18.33 \pm 0.62	20 \pm 1.58	0	83.99
<i>Streptococcus pyogenes</i>	7.66 \pm 0.94	21 \pm 1.41	0	13.30
<i>Pseudomonas aeruginosa</i>	12.33 \pm 0.62	20 \pm 0.70	0	38
<i>Proteus vulgaris</i>	10.33 \pm 1.17	25 \pm 2.16	0	17.07
<i>Escherichia coli</i>	19.66 \pm 0.23	30 \pm 0.70	0	42.94
<i>Candida albicans</i>	24 \pm 0.20	26 \pm 0.81	0	85.20
<i>Aspergillus niger</i>	18 \pm 0.35	22 \pm 0.70	0	66.94

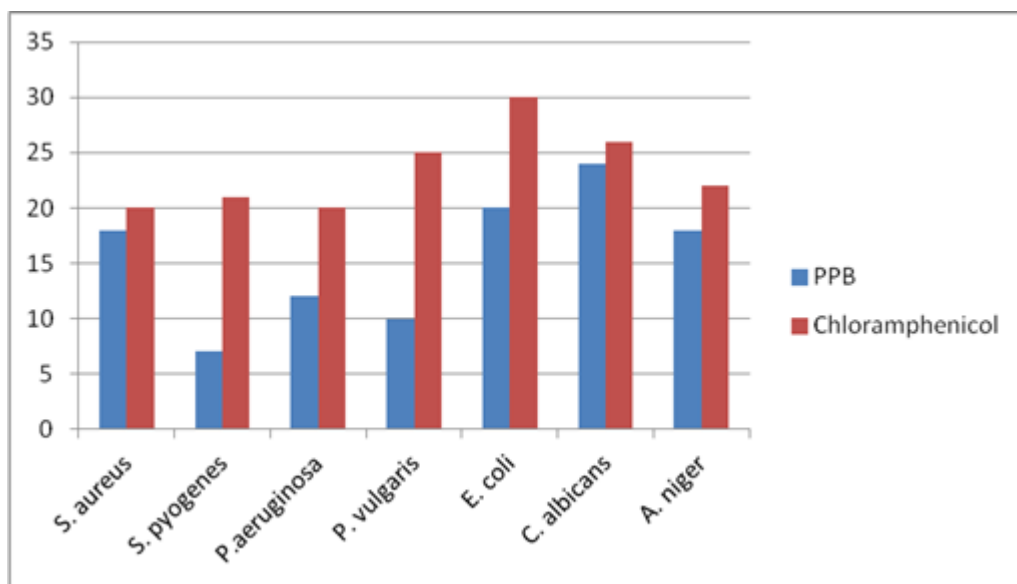


Figure 1. Antimicrobial activity of PPB

As it can be seen from the Table 3, PPB showed antibacterial activity against *S. aureus* and *S. pyogenes* with inhibition zones of 8 and

18 mm, respectively. The most potent activity was observed against *S. aureus*. Similarly, PPB also showed high antibacterial activity against gramnegative bacteria with inhibition zones between 12 and 20 mm. As shown in Table 3, PPB showed antifungal activity against *C. albicans*, with an inhibition zone of 24 mm. The tested compound also showed antifungal activity against *A. niger* with an inhibition zone of 18 mm.

The results of the antimicrobial activity of PPB were compared with those of cloramfenicol and they are gathered in Table 3. The maximum relative percentage of inhibition was exhibited against *C. albicans* (85.20 %) followed by *S. aureus* (83.99 %), *A. niger* (66.94 %), *E. coli* (42.94 %), *P. aeruginosa* (38 %), *P. vulgaris* (17.07 %), and *S. Pyogenes* (13.30 %), respectively.

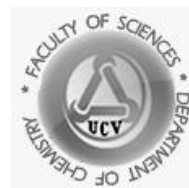
CONCLUSIONS

Some azoderivatives have antimicrobial activity due to the presence of the azo group. 4-Phenylazo-phenoxyacetic acids having methyl substituent exhibit good antibacterial activity. The tested 4-phenyldiazenyl-4'-[(4-chlorobenzyl)oxy]biphenyls showed antibacterial activity. Four 4-[(4-chlorobenzyl)oxy]azobenzene isomers inhibit the growth of *C. albicans*. PPB presents the highest antibacterial activity against *S. aureus*.

References

1. S. Radu, C. Șarpe-Tudoran, A. Jianu, G. Rău, *Rev. Roum. Chim.*, 43 (1998) 735.
2. A. Moanță, B. Tutunaru, P. Rotaru, *J. Therm. Anal. Calorim.*, 111 (2013) 1273.
3. E. Ispir, *Dyes Pigment.*, 82 (2009) 13.
4. S. Alghool, H. F. Abd El-Halim, A. Dahshan, *J. Mol. Struct.*, 983 (2010) 32.
5. H. Xu, X. Zeng, *Bioorg. Med. Chem. Lett.*, 20 (2010) 4193.
6. Z. B. Zhao, H. X. Zheng, Y. G. Wei, J. Liu, *Chinese Chem. Lett.*, 18 (2007) 639.

7. S. S. Dhaneshwar, M. Kandpal, G. Vadnerkar, B. Rathi, S. S. Kadam, *Eur. J. Med. Chem.*, 42 (2007) 885.
8. M. Tonelli, V. Boido, C. Canu, A. Sparatore, F. Sparatore, M. S. Paneni, M. Fermeglia, S. Pricl, P. La Colla, L. Casula, C. Ibba, D. Collu, R. Loddo, *Bioorg. Med. Chem.*, 16 (2008) 8447.
9. P. Frid, S. V. Anisimov, N. Popovic, *Brain Res Rev.*, 53 (2007) 135–60.
10. A. Moanță, S. Radu, *Rev. Roum. Chim.*, 54 (2009) 151.
11. A. Moanță, S. Radu, *Rev. Chim. (Bucharest)*, 59 (2008) 708.
12. S. Radu, M. Băniceru, A. Jianu, G. Rău, *Rev. Roum. Chim.*, 46 (2001) 63.
13. A. Moanță, *J. Chi. Chem. Soc.*, 59 (2014) 2275.
14. A. Moanță, S. Radu, G. Rău, *Rev. Chim. (Bucharest)*, 58 (2007) 229.
15. S. Radu, A. Moanță, G. Rău, *Rev. Chim. (Bucharest)*, 52 (2001) 619.
16. A. Moanță, C. Ionescu, M. Dragoi, B. Tutunaru, P. Rotaru, *J. Therm. Anal. Calorim.*, 120 (2015) 1151.
17. S. M. Abdallah, H. A. Hefny, *Turk J Chem.*, 35 (2011) 463.
18. D. S. Dogruer, S. Urlu, T. Onkol, B. Ozcelik B, M. F. Sahin, *Turk. J. Chem.*, 34 (2010) 57.
19. A. M. A. Hamil, M. M. El-ajaily, H. A. A. Bogdadi, *Int. J. Pharm. Tech. Res.*, 1 (2009) 1714.
20. E. Grandmougin, H. Freimann, *Zur. J. Pr. Chem.*, 78 (1909) 384.



Investigating the coordination manner of a heterocyclic thioamide to Pt(II) by EHT interpretation of the electronic spectra for both free and coordinated organic ligand

Research article

Liana Simona Sbîrnă^{1}, Sebastian Sbîrnă², Anișoara Oubraham³*

¹ University of Craiova, Faculty of Sciences, Department of Chemistry, Calea București, 107i, Craiova, Romania

² Alro S. A., Strada Pitești, 116, Slatina, Romania

³ National R&D Institute for Cryogenics and Isotopic Technologies - ICIT Rm. Vâlcea, Romania

*e-mail: simona.sbirna@gmail.com

Received: 17.11.2017 / Accepted: 14.12.2017 / Published: 22.12.2017

Abstract

The present paper reports the results of a quantum-mechanical study that consists in interpreting the electronic spectra exhibited by a heterocyclic thioamide (namely 3-thiobenzoylamino-dibenzofuran) and its complex compound formed with Pt(II) by means of EHT (Extended Hückel Theory) calculation.

As a result of investigating the energies and EHT expressions of the molecular orbitals in the frontier zone, we can decide which of the heteroatoms contained in the organic molecule are the ones involved in the coordination and, therefore, which is the real structural formula of the complex compound.

Keywords: heterocyclic thioamides, Pt(II) complex compounds, electronic spectra, frontier molecular orbitals, EHT calculation

1. INTRODUCTION

Particular attention has been paid lately to the branch of coordinative chemistry involving the complex compounds formed by a platinum ion with heterocycles that can act as ligands (therefore using heteroatoms as electron donors [1-4]).

Such complex compounds have been synthesized and then structurally investigated using elemental analysis, followed by regular physical-chemical analyses (such as molar conductivity and magnetic behavior measurements, mass spectrometry, infrared and electronic spectroscopy [1-4]).

This paper deals with a complex compound formed by a d^8 transition metal ion (divalent platinum) with a molecule (heterocyclic thioamide) that can act as bidentate ligand, but it is not obvious which pair of heteroatoms it involves in the coordination. Consequently, the purpose of the present work is to establish, by quantum-mechanical means, the actual coordination manner.

2. MATERIALS AND METHODS

2.1. *Materials*

Platinum dichloride 98 % (Sigma-Aldrich) was used to react with double recrystallized 3-thiobenzoylamino-dibenzofuran. We also used ethanol, diethyl ether and acetone, all these chemicals being of analytical grade.

The elemental analysis was performed on a Perkin Elmer 2380 (USA) analyzer. The magnetic susceptibility of the complex was investigated using a Holmarc Gouy's Method Apparatus, Model HO-ED-EM-08 (India), whereas its electrical conductivity was measured on a Radelkis OK-102/1 (Hungary) conductivity meter, for which the cell constant is 0.9 cm^{-1} .

Both electronic spectra were performed in 10^{-3} M acetone solutions, with an Ocean Optics (UK) spectrophotometer.

The software that we have used to simulate the molecular structures was HyperChem 8.0.10 program (trial version [5]).

2.2. Methods

The heterocyclic thioamide (3-thiobenzoylamino-dibenzofuran) was obtained as described by Florea [6]. Then, its complex compound with Pt(II) has been prepared following the method proposed by Jensen and Nielsen [7].

An ethanolic solution (0.02 M) of the thioamide was added – dropwise and continuously stirring – to an aqueous solution of platinum dichloride (also 0.02 M) in a 1:1 ratio.

After gently stirring for one hour, the reaction vessel was left for three more hours to settle at room temperature. Then, the product was finally filtered off, washed with ethanol and diethyl ether and dried under reduced pressure.

The isolated complex compound fine crystalline precipitate was washed with diethyl ether and air dried.

3. RESULTS AND DISCUSSION

3.1. Preliminary statements

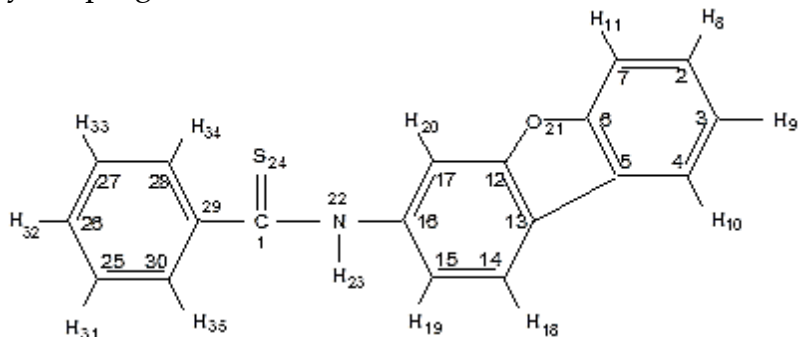
The elemental analysis has shown that the complex compound contained (besides the metal ion) only one molecule of organic ligand and two chloride ions.

This statement is sustained by the fact that it appears to be a non-electrolyte and, moreover, a diamagnetic compound.

3.2. Structure of the ligand and complex compound

The structure of the free ligand is the one shown below. As we have written before, the software that used to simulate it was HyperChem 8.0.10 (trial version [5]).

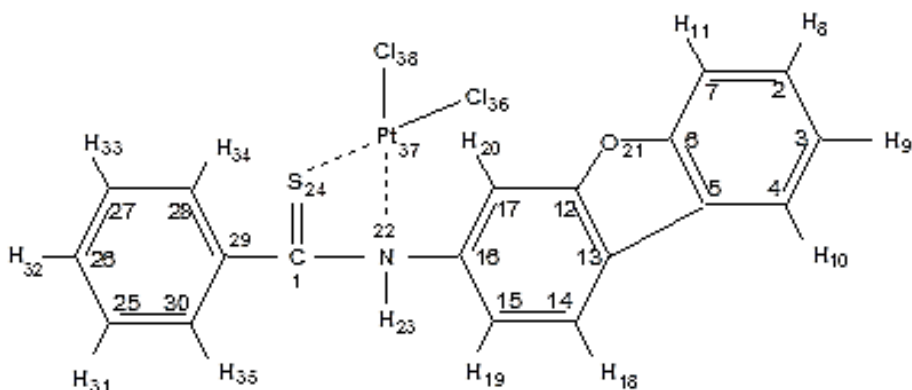
The numbering of the atoms was maintained exactly the one given by the program.



3-thiobenzoylamino-dibenzofuran (denoted as L)

The ligand will be denoted as L in what follows.

The structure of the complex compound, suggested by the preliminary facts earlier presented is the one below.



[Pt(II)LCl₂]

The numbering for all the atoms in the ligand was kept as before, the metal ion and both the chloride ions being also numbered by the HyperChem software [5].

3.3. Performing the EHT calculation

Both molecular structures have been optimized by using the Molecular Mechanics approach (MM⁺).

In order to perform the EHT (Extended Hückel Theory) interpretation, the cartesian coordinates of the atoms corresponding to the bond lengths and angles obtained have been used as input data for ICONC program [8], an improved version of Hoffmann's ICON which was proposed by Calzaferri and Brände.

Within this software, the VSIP parameters were used, as proposed by Gray [9].

The output data of ICONC are the mixing coefficients showing the involvement of each atomic orbital (AO) in every molecular orbital (MO).

The EHT calculation was performed without iteration upon charge and configuration, as the EHT practice shows that the results thus acquired are more reliable if the electronic transitions between MO levels are compared with the spectral ones.

3.3. Frontier molecular orbital energy levels

The energy levels of the frontier molecular orbitals are indicated by the Extended Hückel ICONC program.

Table 1. Frontier molecular orbital energy levels for the ligand, L

Molecular orbital	Electron occupation	Energy (eV)
Ψ_{43}	0	-6.80183
Ψ_{44}	0	-7.19892
Ψ_{45}	0	-7.35523
Ψ_{46}	0	-7.52359
Ψ_{47}	0	-8.44770
Ψ_{48}	0	-10.01689
Ψ_{49}	2	-10.93975
Ψ_{50}	2	-11.40118
Ψ_{51}	2	-11.44855
Ψ_{52}	2	-11.91661

The energetic values are labeled below for the frontier molecular orbitals of the free ligand (which are denoted by Ψ) and also for the ones of the Pt(II) complex compound (which are denoted by Ψ') – as seen from tables 1 and 2.

Table 2. Frontier molecular orbital energy levels for [Pt(II) LCl₂]

Molecular orbital	Electron occupation	Energy (eV)
Ψ'_{48}	0	-6.83538
Ψ'_{49}	0	-7.22834
Ψ'_{50}	0	-7.26227
Ψ'_{54}	0	-8.89248
Ψ'_{55}	2	-9.50260
Ψ'_{56}	2	-9.81242
Ψ'_{57}	2	-9.82219
Ψ'_{58}	2	-11.60287
Ψ'_{59}	2	-11.99239

3.4. Frontier molecular orbital expressions

The expressions of the frontier molecular orbitals are obviously not directly given by the Extended Hückel ICONC program, but we could write them by using the mixing coefficients indicated as its output data (keeping only the significant ones, *i.e.*, the ones exceeding the value 0.1).

For the free ligand, the frontier molecular orbital expressions, containing only the most significant mixing coefficients, are given below:

$$\Psi_{43} \approx -0.3029C_2(x) - 0.2653C_2(y) + 0.1409C_2(z) + 0.4514C_3(x) + 0.3947C_3(y) - 0.2063C_3(z) - 0.2270C_4(x) - 0.1996C_4(y) - 0.1883C_5(x) - 0.1710C_5(y) + 0.4069C_6(x) + 0.3646C_6(y) - 0.1966C_6(z) + 0.1909C_{12}(x) + 0.1897C_{12}(y) - 0.2604O_{21}(x) - 0.2494O_{21}(y)$$

$$\Psi_{44} \approx 0.5963C_{25}(y) + 0.2574C_{25}(z) + 0.3560C_{26}(x) + 0.1747C_{27}(y) - 0.3762C_{27}(z) + 0.1797C_{28}(x) + 0.4747C_8(z) - 0.1902C_{29}(z) - 0.4524C_{30}(y) - 0.1731C_{30}(z)$$

$$\begin{aligned}
\Psi_{45} &\approx -0.2712S_{24}(y)+0.2301S_{24}(z)+0.3397C_1(y)-0.3904C_1(z)+0.1734C_2(x)+ \\
&\quad +0.1513C_2(y)-0.2785C_4(x)-0.2467C_4(y)+0.1938C_5(x)+0.1629C_5(y)- \\
&\quad -0.2774C_7(x)-0.2446C_7(y)-0.2477N_{22}(y)+0.1800N_{22}(z)-0.1835C_{25}(y)- \\
&\quad -0.1610C_{25}(z)+0.1975C_{28}(y)-0.1515C_{29}(z)+0.2835C_{30}(z) \\
\Psi_{46} &\approx -0.1867C_1(y)+0.2067C_1(z)-0.2422C_4(x)-0.2153C_4(y)-0.2425C_7(x)- \\
&\quad -0.2086C_7(y)-0.3337C_{12}(x)-0.3373C_{12}(y)+0.1535C_{12}(z)+ \\
&\quad +0.2125C_{14}(x)+0.2974C_{14}(y)-0.1855C_{14}(z)+0.2617C_{17}(x)+ \\
&\quad +0.2764C_{17}(y) \\
\Psi_{47} &\approx -0.2040S_{24}(y)+0.2216S_{24}(z)+0.2031C_1(y)-0.2756C_1(z)-0.2149C_2(x)- \\
&\quad -0.1871C_2(y)+0.2167C_4(x)+0.1870C_4(y)-0.1795C_5(x)+0.1553C_7(x)- \\
&\quad -0.1816C_{13}(x)-0.1885C_{13}(y)+0.2884C_{14}(x)+0.3857C_{14}(y)-0.2438C_{14}(z)- \\
&\quad -0.1980C_{16}(x)-0.2738C_{16}(y)+0.2845C_{17}(x)+0.3327C_{17}(y) \\
\Psi_{48} &\approx 0.5406C_{26}(x)-0.2417C_{26}(y)-0.1748C_{27}(y)+0.5655C_{27}(z)-0.2350C_{29}(y)- \\
&\quad -0.2029C_{29}(z)+0.2263C_{30}(y)+0.1848H_{31}(s)+0.1960H_{32}(s)+0.1766H_{33}(s)+ \\
&\quad +0.1760H_{34}(s) \\
\Psi_{49} &\approx 0.8308S_{24}(x)-0.3231S_{24}(y) \\
\Psi_{50} &\approx 0.2356N_{22}(x)+0.2585N_{22}(y)+0.1920S_{24}(x)-0.2595S_{24}(y)+0.4967S_{24}(z)+ \\
&\quad +0.2004C_{13}(x)-0.1952C_{15}(y)+0.2486C_{26}(x)-0.2525C_{27}(z)+0.1787C_{29}(x)+ \\
&\quad +0.1621C_{29}(z)+0.1852C_{30}(y) \\
\Psi_{51} &\approx -0.4113C_{26}(x)+0.2162C_{26}(y)+0.3563C_{27}(z)-0.2494C_{29}(x)-0.2619C_{29}(z)- \\
&\quad -0.2874C_{30}(y) \\
\Psi_{52} &\approx 0.4860O_{21}(x)+0.4581O_{21}(y)-0.2165O_{21}(z)+0.1891C_3(x)+0.1547C_3(y)- \\
&\quad -0.1925C_7(x)-0.1797C_7(y)-0.1744C_{13}(x)+0.2282C_{15}(y)-0.1506C_{17}(x)- \\
&\quad -0.2284C_{17}(y)
\end{aligned}$$

For the complex compound, the frontier molecular orbital expressions, also containing only the most significant mixing coefficients, are the following:

$$\begin{aligned}
\Psi'_{48} &\approx 0.2577C_2(y)+0.4103C_3(y)+0.1937C_3(x)-0.2207C_4(y)-0.1469C_5(y)+ \\
&\quad +0.3829C_6(y)-0.1810C_6(x)-0.2097C_{12}(x)+0.4411C_{12}(y)-0.2773C_{14}(y)+ \\
&\quad +0.3600C_{15}(y)-0.1456C_{16}(y)-0.2686C_{17}(y)+0.1714O_{21}(x)-0.3613O_{21}(y) \\
\Psi'_{49} &\approx 0.1886C_3(x)-0.3997C_3(y)-0.1818C_4(x)+0.3828C_4(y)+0.1959C_6(x)- \\
&\quad -0.4151C_6(y)-0.1672C_7(x)+0.3526C_7(y)-0.1730C_{12}(x)+0.3638C_{12}(y)+ \\
&\quad +0.1537C_{14}(x)-0.3182C_{14}(y)-0.1639C_{15}(x)+0.3312C_{15}(y)+0.1502C_{17}(x)- \\
&\quad -0.3193C_{17}(y) \\
\Psi'_{50} &\approx 0.4958C_{30}(x)+0.3090C_{30}(y)-0.5282C_{25}(x)-0.3393C_{25}(y)+0.4419C_{27}(x)+
\end{aligned}$$

$$\begin{aligned}
& +0.2829C_{27}(y)-0.4759C_{28}(x)-0.3089C_{28}(y) \\
\Psi'_{54} \approx & -0.8364Ni_{37}(xy)-0.2863Ni_{37}(x^2-y^2)+0.2796Ni_{37}(z^2)+0.1721N_{22}(y)+ \\
& +0.2021Cl_{36}(y)+0.1819Cl_{38}(y) \\
\Psi'_{55} \approx & -0.6748Ni_{37}(x^2-y^2)-0.4288Ni_{37}(xz)+0.2134Ni_{37}(xy)-0.3301Ni_{37}(xz)+ \\
& +0.2176S_{24}(x)+0.1530S_{24}(y)-0.2040C_1(x)-0.1517Cl_{38}(x) \\
\Psi'_{56} \approx & -0.6706Ni_{37}(yz)-0.4268Ni_{37}(xz)-0.2019Ni_{37}(xy)-0.5523Ni_{37}(z^2)+ \\
& +0.1687S_{24}(x) \\
\Psi'_{57} \approx & -0.5926Ni_{37}(xz)-0.3225Ni_{37}(yz)-0.2476S_{24}(x)-0.1823S_{32}(y)+ \\
& +0.3874C_1(x)+0.2721C_1(y)-0.2281C_{30}(x)+0.2466C_{27}(x)+0.1593C_{27}(y)- \\
& -0.2171C_{28}(x) \\
\Psi'_{58} \approx & 0.7578S_{24}(z)+0.2460S_{24}(y)-0.3751Ni_{37}(z^2)-0.1970Ni_{37}(yz) \\
\Psi'_{59} \approx & 0.6444O_{21}(y)-0.3047O_{21}(x)+0.1504O_{21}(z)+0.2548C_3(y)-0.2056C_5(y)- \\
& -0.2462C_7(y)+0.1729C_{14}(y)+0,1853C_{15}(y)-0,2904C_{17}(y)
\end{aligned}$$

Using these expressions, the assignment of the electronic transitions for both the free and coordinated heterocyclic thioamide can be made, with a good probability [10].

3.5. Assigning the electronic transitions of the free and coordinated ligand

The electronic spectra recorded for 3-thiobenzoylamino-dibenzofuran (L) and for its complex compound formed with Pt(II) – together with two chloride ions – are shown in figures 1 and 2.

These spectra were compared with each other, taking into account the expressions previously found through the quantum-mechanical study which was earlier conducted.

The most probable assignment of the electronic transitions of the free and coordinated ligand are presented in tables 3 and 4.

As a result of investigating the energies and the EHT expressions of the molecular orbitals in the frontier zone, we could decide which of the hetero-atoms contained in the organic molecule are the ones through which the coordination is realized.

Therefore, we might be able to decide if the proposed structural formula is the real one for the complex compound [10].

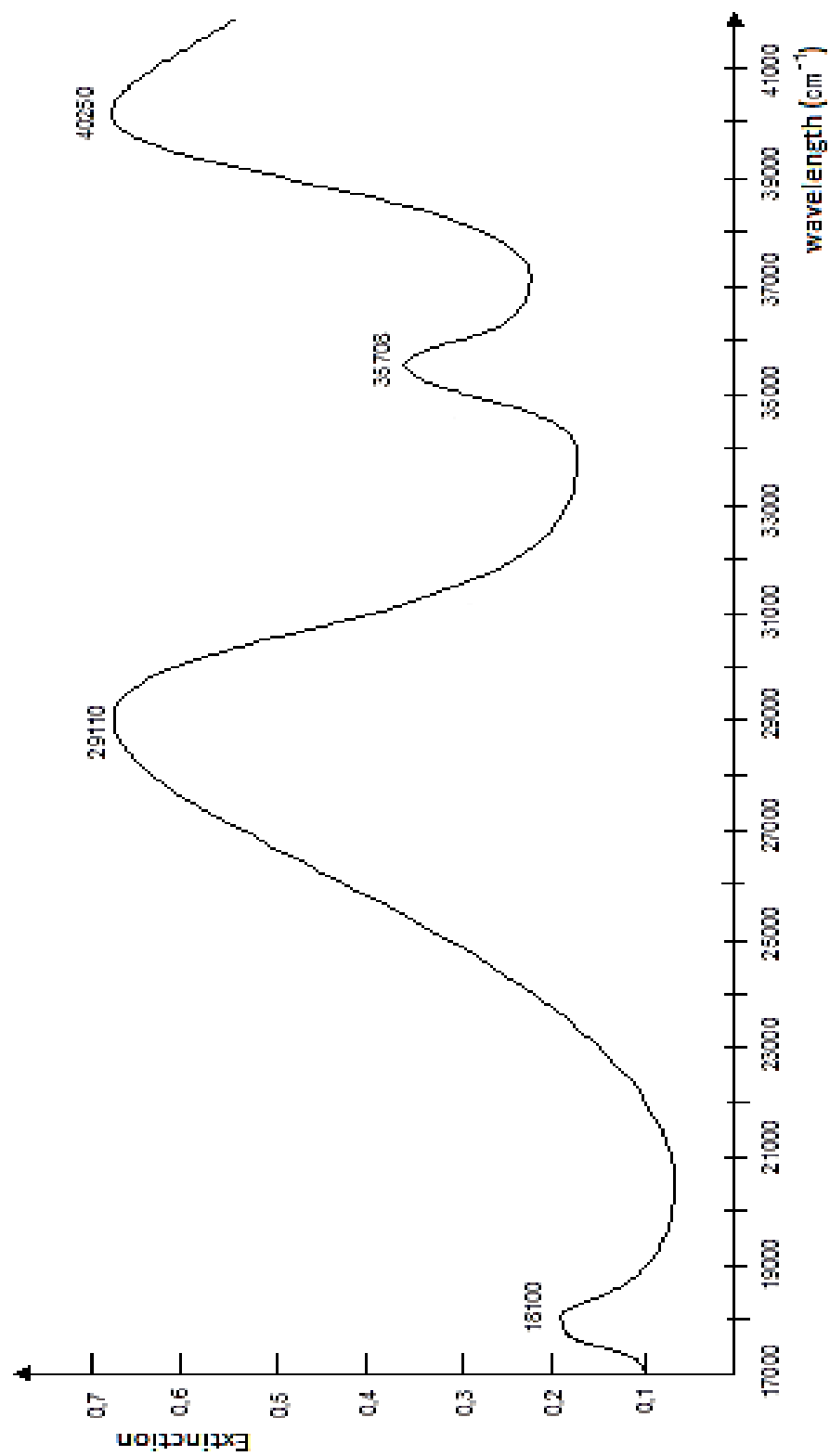


Figure 1. The electronic spectrum of the ligand, L (3-thiobenzoylamino-dibenzofuran)

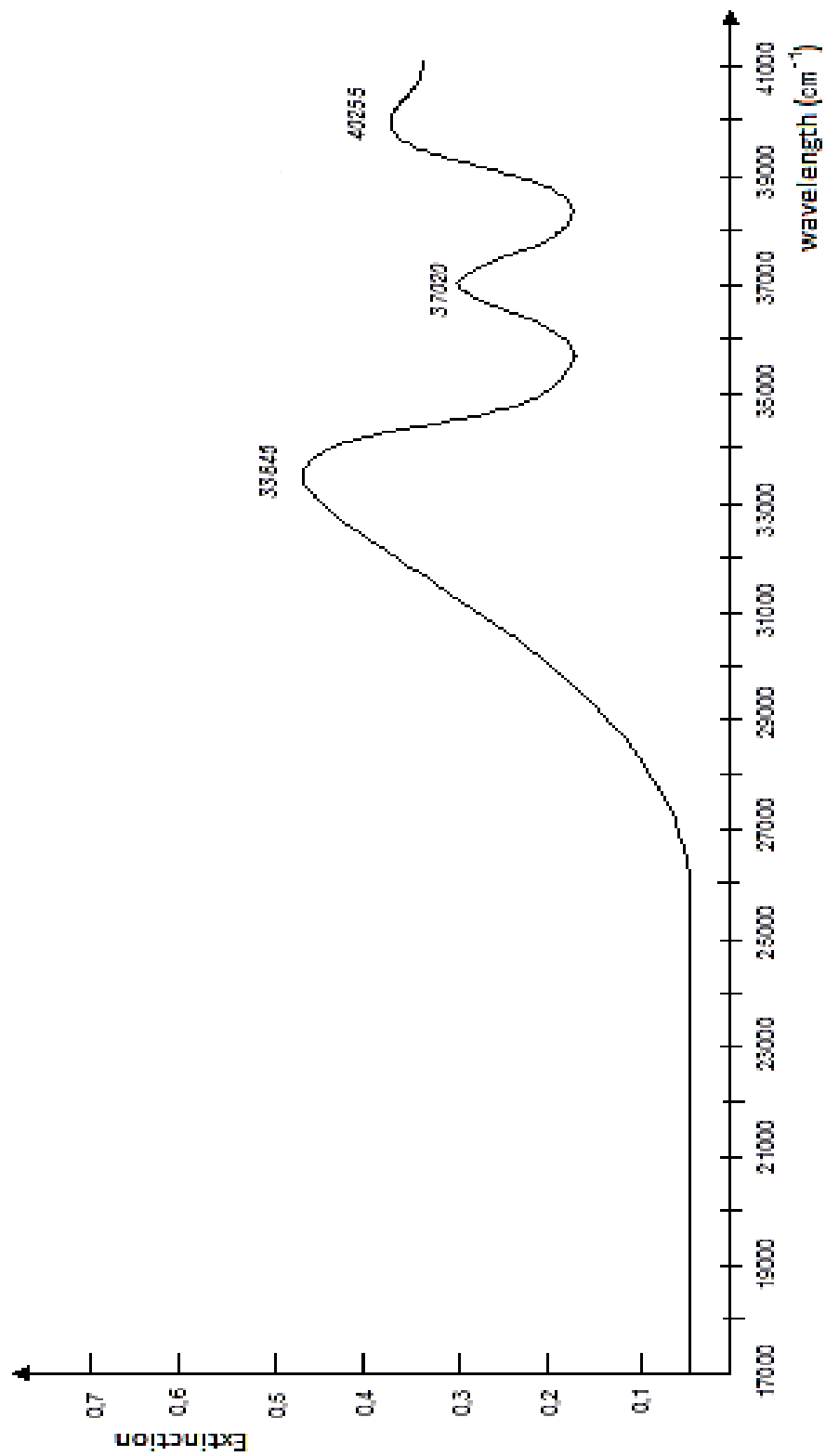


Figure 2. The electronic spectrum of the complex compound, [Pt(II)LCl₂]

Table 3. EHT assignment for the electronic transitions of the free organic ligand

	EHT electroni c transition	calculated wavelengt h (cm ⁻¹)	calculated energy (eV)	experiment al wavelength (cm ⁻¹)	experiment al energy (eV)
a	$\Psi_{49} \rightarrow \Psi_{47}$	20101	2.49205	18110	2.24398
	$\Psi_{49} \rightarrow \Psi$	27555	3.41616		
b	Ψ_{46}	28912	3.58452	29110	3.60898
	$\Psi_{49} \rightarrow \Psi$	30173	3.74083		
	Ψ_{45}				
	$\Psi_{49} \rightarrow \Psi$				
	Ψ_{44}				
c	$\Psi_{49} \rightarrow \Psi$	33376	4.13792	35708	4.42698
	Ψ_{43}				
d	$\Psi_{52} \rightarrow \Psi$	41256	5.11478	40250	4.99008
	Ψ_{43}				

Table 4. EHT assignment for the electronic transitions of the coordinated ligand

	EHT electroni c transition	calculated wavelengt h (cm ⁻¹)	calculated energy (eV)	experiment al wavelength (cm ⁻¹)	experiment al energy (eV)
a	-	-	-	-	-
b	$\Psi'_{58} \rightarrow \Psi'_{50}$	35011	4.34060	33846	4.19613
	$\Psi'_{58} \rightarrow \Psi'_{49}$	35285	4.37453		
c	$\Psi'_{58} \rightarrow \Psi'_{48}$	38452	4.76749	37020	4.58964
d	$\Psi'_{59} \rightarrow \Psi'_{48}$	41596	5.15701	40255	4.99070

This assignment of the electronic transitions of the free and coordinated ligand shows that the oxygen atom in the heterocycle has nothing to do with the coordination, which therefore only involves the other two heteroatoms present in the molecule of the ligand [10].

4. CONCLUSION

The electronic spectrum of the complex was compared to the one of the free organic ligand, a quantum-mechanical study having been then conducted with this particular purpose, by performing EHT (Extended Hückel Theory) calculation. More specifically, this study started by computationally simulating the structures for both free and coordinated organic ligand within the HyperChem 8.0.10 program, which offers information about the energies of the molecular orbitals. Then, the expressions of the molecular orbitals in the frontier zone were written (by taking into account only the significant mixing coefficients), in order to decide how to attribute the electronic transitions appearing in the two spectra. By corroborating the differences and similarities between them, we made the assumption that coordination involves indeed the nitrogen and sulfur atoms from the thioamidic group of the ligand, so the structural formula is right.

References

1. L. G. Golubyatnikova, R. A. Khisamutdinov, S. A. Grabovskii, N. N. Kabal'nova, Yu. I. Murinov, *Russian Journal of General Chemistry*, 87/1 (2017) 117.
2. A. Gouranourimi, M. Ghassemzadeh, S. Bahemmat, B. Neumüller, R. Tonner, *Monatshefte für Chemie (Chemical Monthly)* 146/1 (2015) 57.
3. S. J. Choi, J. Kuwabara, Y. Nishimura, T. Arai, T. Kanbara, *CSJ Journals, Chemical Letters*, 41/1 (2012) 65.
4. S. S. Kandil, S. M. A. Katib, N. H. M. Yarkandi, *Transition Metal Chemistry*, 32/6 (2007) 791.
5. <https://en.freedownloadmanager.org/Windows-PC/HyperChem.html>
6. S. Florea, *Revue Roumaine de Chimie*, 39 (1994) 1138.
7. K. A. Jensen, P. H. Nielsen, *Acta Chemica Scandinavica*, 20 (1966) 597.
8. G. Calzaferri, M. Brände, *QCPE Buletin*, 12 (1992) 73.
9. H. B. Gray, *Electrons and Chemical Bonds*, W. A. Benjamin Inc., New York (1965).
10. L. S. Sbîrnă, S. Sbîrnă, C. I. Lepădatu, V. Mureşan, N. Mureşan, *Journal of Indian Chemical Society*, 79/5 (2002) 409.



Total phenolic content and antioxidant activity in leaves of six *Salix* genotypes

Research article

*Cristina Băbeanu*¹, *Ana Maria Dodocioiu*^{2,*}

¹University of Craiova, Faculty of Sciences, Department of Chemistry, Calea Bucuresti, 107i, Craiova, Romania

²University of Craiova, Faculty of Horticulture, A.I. Cuza Street 13, Craiova, Romania

*E-mail: anadodocioiu@gmail.com

Received: 13.11.2017 / *Accepted:* 11.12.2017 / *Published:* 22.12.2017

Abstract

The *Salix* extracts are used in traditional medicine having important pharmacological properties. Due to the fact that the beneficial effects are explained by the content in many bioactive phytochemicals, the purpose of this paper is to evaluate in comparison the total phenolic content, the flavonoids content and antioxidant activity in leaves of six *Salix* clones in order to select the most valuable genotypes as source of natural antioxidants.

The total phenolic content and the flavonoids content were determined by colorimetric methods and the antioxidant activity was evaluated by DPPH radical and ABTS cation radical scavenging assay. The obtained results show that all the studied genotypes show a high total phenolic content and significant antioxidant activity and recommend their use in new therapeutic drugs as new sources of phenolic compounds and natural antioxidants.

Keywords: *Salix* sp., phenolic compounds, flavonoids, antioxidant activity

1. INTRODUCTION

The *Salix* extract has a long history as a traditional remedy for the treatment of fever, pain and inflammation, the beneficial effects being associated with high salicylate content and salicylic acid precursors [1, 2]. These precursors are metabolized in the body to salicylic acid, a well-known compound for its anti-inflammatory and analgesic properties and its protective role in cardiovascular disease and some type of cancers [3]. Other phytochemicals present in *Salix* extracts are: salicortin, salicin, salicylic alcohol, cinnamic acid derivatives, myricetin, kaempferol, quercetin, rutin, luteolin and condensed tannins [4, 5].

Only the concentration in salicylates and salicylic alcohol derivatives does not explain alone the therapeutic potential of *Salix* extract and many papers suggest that other polyphenolic compounds are responsible for biological activity and clinical effects [6].

Phenolic compounds have anti-inflammatory, anti-atherogenic, anti-microbial and anti-carcinogenic properties [7, 8]. These natural compounds have been found to be strong antioxidants against free radicals and other reactive oxygen species.

The purpose of this study is to evaluate the antioxidant activity and content in total phenolic compounds and total flavonoids content in leaves of six *Salix* genotypes grown in the climatic conditions of South West Romania, with high temperature and lack of precipitation.

2. MATERIALS AND METHODS

2.1. *Materials*

The used methanol for the extraction was from Sigma-Aldrich (Germany). Gallic acid, DPPH 1,1-diphenyl-2-picrylhydrazyl, ABTS 2,2'-azino-bis(3-ethylbenzothiazoline-6-sulphonic acid), Trolox 6-hydroxy-2,5,7,8-tetramethylchroman-2-carboxylic acid were obtained from Sigma-Aldrich and Quercetin was purchased from Carl Roth. Folin-Ciocalteu reagent was obtained from Merck (Germany). All the other used chemicals were of analytical grade.

The biological material analyzed consisted of six genotypes of *Salix*, three Romanians: Cozia, 1077, Robisal and 3 Swedish: Tora, Jorr and Olof from a plantation in the Radovan area (N 44°10'05" E 23°36'13") founded by Faculty of Agriculture, University of Craiova [9]. The content in total phenolic compounds, the content of total flavonoid compounds and the anti-oxidant activity were determined in methanolic extract.

2.2. Method

For the determination of total phenolic content, total flavonoid content and antioxidant activity samples were extracted with 80 % aqueous methanol (1:20 w/v) by sonicating for 60 min in a bath sonicator at 24 °C. The resulting slurries were centrifuged at 4000 g for 5 min and the supernatants were collected.

The total phenolics content was determined colorimetric at 765 nm by the Folin Ciocalteu reagent method [10] with some modifications [11]. Gallic acid was used to construct standard curve and the results were expressed as mg GAE g⁻¹ f.w.

Total flavonoids content was determined by colorimetric method [11]. 0.5 mL of the sample extract (diluted 1:10 with methanol) was added to 0.6 mL of 5 % sodium nitrite (NaNO₂) and the mixture was left for 6 min. 0.5 mL of 10 % Al(NO₃)₃ was added, shaken and left to stand for 6 min. Finally, 3.0 mL of the 4.3 % NaOH was added. The mixture was shaken and the absorbance was read at 500 nm after 15 min incubation at room temperature. The total flavonoid concentration was calculated from quercetin calibration curve and expressed as mg quercetin equivalents per gram fresh weight (mg QE g⁻¹ fw.)

DPPH (2,2-diphenyl-1-picrylhydrazyl) radical scavenging assay: The capacity of extracts to reduce the radical 2,2-diphenyl-1-picrylhydrazyl was assessed colorimetric [11] with some modifications. 3 mL of 0.075 mM DPPH methanolic solution was mixed with 50 µL extract (diluted 1:10 with methanol) and vortexed thoroughly. The absorbance of the mixtures was measured at 517 nm after 30 min. A blank reagent was used to study stability of DPPH over the test time. The percentage of

DPPH radical scavenging activity of extracts was evaluated according to the formula:

$$\% \text{ scavenging} = \frac{A_0 - (A_1 - A_s)}{A_0} \times 100 \quad (1)$$

where A_0 is the absorbance of DPPH alone, A_1 is the absorbance of DPPH + extract and A_s is the absorbance of the extract only.

Trolox (T) and ascorbic acid (AsA) were used as standards. The standards calibration curves were plotted as a function of the percentage of DPPH radical scavenging activity. The results were expressed as μmol Trolox equivalents per gram ($\mu\text{mol TE g}^{-1}$ f.w.) and μmol ascorbic acid equivalents per gram ($\mu\text{mol AsA g}^{-1}$ fw) respectively.

ABTS 2,2'-azino-bis(3-ethylbenzothiazoline-6-sulphonic acid) radical cation scavenging activity: The ABTS radical cation scavenging activity of the plant extract was measured colorimetric [12]. ABTS was dissolved in water to a 7 mmol L^{-1} concentration. ABTS radical cation was produced by reacting ABTS stock solution with 2.45 mmol L^{-1} potassium persulfate and allowing the mixture to stand in the dark at room temperature for 12 - 16 h before use. The ABTS radical cation solution was diluted with methanol to an absorbance of 0.70 at 734 nm. $50 \mu\text{L}$ extract (diluted 1:10 with methanol) of the sample was mixed with 2.95 mL of diluted ABTS radical cation solution. After reaction at room temperature for 6 min, the absorbance at 734 nm was measured. Trolox (T) and ascorbic acid (AsA) were used as standards. The standards calibration curves were plotted as a function of the percentage of ABTS radical cation scavenging activity calculated using equation 1. The results were expressed as μmol Trolox equivalents per gram ($\mu\text{mol TE g}^{-1}$ fw) and μmol ascorbic acid equivalents per gram ($\mu\text{mol AsA g}^{-1}$ fw) respectively. All determinations were performed in triplicate, and all results were calculated as mean.

3. RESULTS AND DISCUSSION

3.1. Total phenolic content and total flavonoids content

The results obtained for total phenolic content vary with the investigated genotype (figure 1) and ranged from 18.968 mg GAE g⁻¹ f.w. (Robisal) to 32.4 mg GAE g⁻¹ f.w. (Tora) in the order: Tora> Olof> Jorr> Cozia> 1077> Robisal. It is found that in Swedish clones the content in total phenolic content is higher than that obtained for the Romanian clones.

The results of the total flavonoids content for the investigated clones varies between 9.44 mg QE g⁻¹ (Robisal) and 17.94 mg QE g⁻¹ (Olof) as follows: Olof > Jorr> Cozia> Tora> 1077> Robisal (Figure 1). Flavonoids compounds represent a higher percentage related to total phenolic content and varied between 46.17 % (Tora) and 66.34 % (Jorr) genotype.

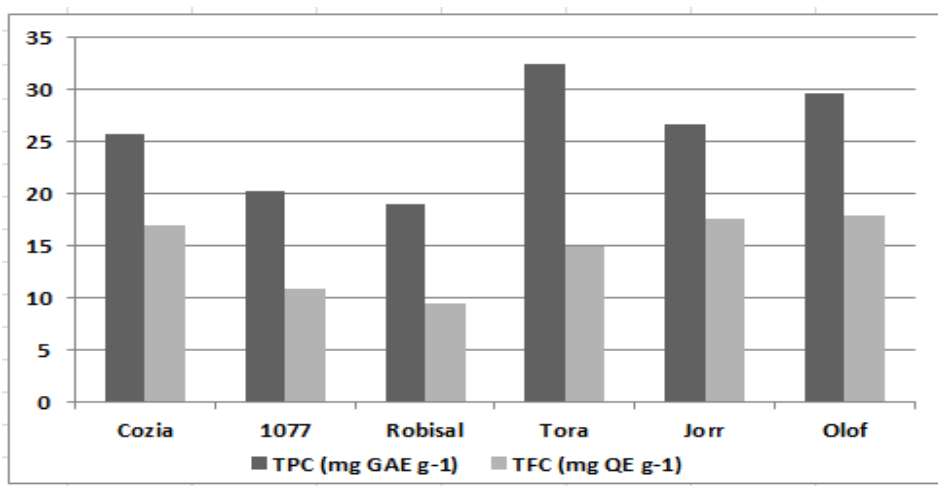


Figure 1. Total phenolic content (TPC) and total flavonoids content (TFC) in leaves of investigated *Salix* genotypes

Numerous papers present the content of phenolic compounds in various organs of *Salix* plants [13, 14]. Identification and quantification in water leaves extract of the individual phenols by HPLC showed that myricetin and catechin were the most abundant flavonols while the

major flavones were luteolin and apigenin and their derivatives [15]. Other phenolic compounds identified are gallic acid, p-coumaric acid, vanillin and caffeic acid and flavonoids: epigallocatechin gallate, rutin, kaempferol and quercetin [13, 16].

Focusing interest on content in phenolic compounds is due to the fact that they possess antioxidant properties [17] which can play an important role in scavenging free radicals, quenching singlet oxygen, or decomposing peroxides and which can explain their health protecting activity [18]

3.2. Antioxidant activity

Antioxidant activity can be determined by various methods that differ in terms of their assay principles and experimental conditions. In this work antioxidant activity of leaves extract was evaluated by two methods: DPPH (2,2-diphenyl-1-picrylhydrazyl) radical and ABTS (2,2'-azino-bis- (3-ethylbenzothiazoline-6-sulfonic acid) cation radical scavenging assay, which are the most commonly accepted. The results were calculated using Trolox (6-hydroxy-2,5,7,8-tetramethylchroman-2-carboxylic acid) and ascorbic acid standards.

The results obtained for antioxidant activity vary with the investigated *Salix* genotype (Figure 2 and Figure 3).

All *Salix* extracts exhibited strong DPPH radical scavenging activity. The values of DPPH radical scavenging activity ranged from 141.75 $\mu\text{mol TE g}^{-1}$ (respectively 101.99 $\mu\text{mol AsA g}^{-1}$) for 1077 genotype to 364.33 $\mu\text{mol TE g}^{-1}$ (respectively 249.85 $\mu\text{mol AsA g}^{-1}$) for Cozia genotype and decreased as follows: Cozia > Tora > Olof > Jorr > Robisal > 1077.

The studied extracts were also measured and compared for their free radical scavenging activities against ABTS radical cation. Results are presented in figure 2 and figure 3. All results showed significant ABTS radical cation scavenging activity.

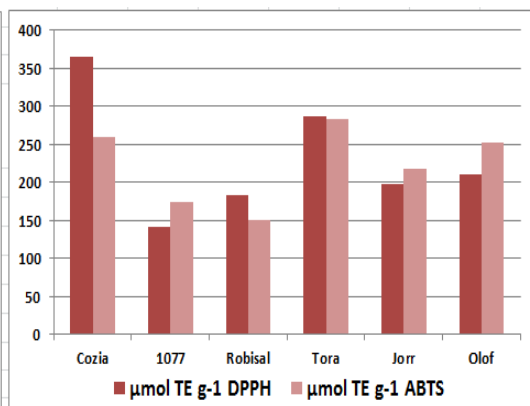
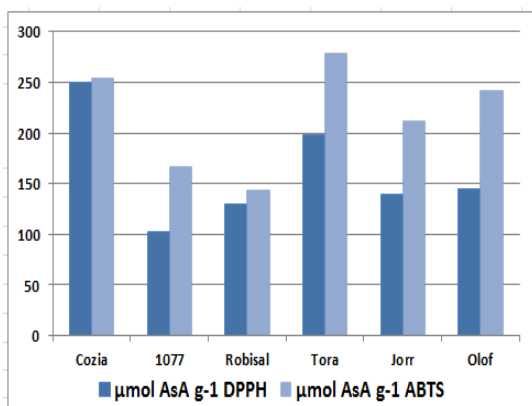


Figure 2. DPPH radical and ABTS radical cation scavenging activities calculated with ascorbic acid standard

Figure 3. DPPH radical and ABTS radical cation scavenging activities calculated with Trolox standard

The values of ABTS radical cation scavenging activity for samples ranged from 150.16 $\mu\text{mol TE g}^{-1}$ (respectively 143.8 $\mu\text{mol AsA g}^{-1}$) for Robisal genotype to 283.73 $\mu\text{mol TE g}^{-1}$ (respectively 278.8 $\mu\text{mol AsA g}^{-1}$) for Tora genotype and decreased as follows: Tora > Cozia > Olof > Jorr > 1077 > Robisal.

The results obtained by ABTS method differ from the results of the DPPH assay. The different results from two methods might be due to different reaction kinetics between phenol and DPPH radical as well as ABTS radical cation over a similar range of concentrations.

Radical scavenging activities are very important due to the role of free radicals in biological systems. These free radicals in excess damage various biomolecules, such as DNA, proteins, lipids and carbohydrates causing many degenerative diseases [19, 20]. The role of antioxidants is to scavenge and inhibit the reactions of free radicals and protect the cell against oxidative damage.

The beneficial effects of Salix extracts proven in numerous clinical studies are explained due to significant antioxidant activity and high content of phenolic and flavonoid compounds. In a study that determines antioxidant activity in bark, catkins and leaves extracted into solvents of increasing polarity it is showed that the highest antioxidant activity was observed in the ethanolic extract of bark followed by the

aqueous leaf extract [13]. The *Salix* leaves also have a high enzymatic antioxidant activity plays a key role in the scavenging and regulation of the level of reactive oxygen species [21, 22].

A strong positive correlation has been observed between the ABTS radical cation scavenging activity and total phenols content ($r=0.93$) and between the ABTS radical cation scavenging activity and total flavonoids content ($r=0.78$). This is explained by the fact that the studied compounds, phenols and flavonoids, are powerful antioxidants due to their ability to scavenge free radicals. A similar relationship ($r=0.77$) was also obtained between total phenol content and total flavonoids content.

Research has reported that there is no significant correlation between salicin and antioxidant activity in different organs of the plant [6, 13]. Commercial salicin as well as acetyl salicylic acid did not show any free radical scavenging activity which also indicates once more that the antioxidant activity of willow leaf extracts is due to phenolic compounds.

4. CONCLUSIONS

The analyzed biochemical indices show a dependency with the investigated genotypes and the obtained results recommend all analyzed genotypes as having high phenolic content and significant antioxidant activity.

The Swedish clones show the highest content in phenolic compounds and flavonoid compounds while the highest antioxidant activity is recorded for Cozia and Tora genotypes.

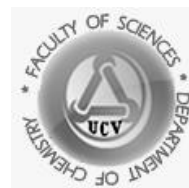
Strong positive correlations have been observed when ABTS radical cation scavenging activity were compared with total phenolics compounds content and total flavonoids content indicating that these compounds are responsible for the antioxidant activity.

This study recommends the use of investigated willow clones as new sources of phenols and natural antioxidants for new therapeutic drugs.

References

1. T. Hedner, B. Everts, *Clin Rheumatol.*, 17 (1998) 17.
2. R. R. Chhetree, G. K. Dash, S. Mondal, R. Parhi, *Int. J. Drug Dev. Res.*, 2 (2010) 799
3. J. G. Mahdi, A. J. Mahdi, A. J. Mahdi, I. D. Bwen, *Cell Prolif.*, 39 (2006) 147.
4. L. Poblocka-Olech, A. M. Van Nederkassel, Y. Van der Heyden, M. Krauze-Baranowska, D. Glod, T. Baczek, *J Sep Sci.*, 30 (2007) 2958.
5. H. Hussain, A. Badawy, A. Elshazly, A. Elsayed, K. Krohn, M. Riaz, B. Schulz, *Rec. Nat. Prod.*, 5 (2011) 133.
6. A. Nahrstedt, M. Schmidt, R. Jaggi, J. Metz, M. Khayyal, *Wien Med Wochenschr.*, 157 (2007) 348.
7. A. Michalak, *Polish J. Of Environ. Stud.*, 15 (2006) 523.
8. J. H. Yoon, S.J. Baek, *Yonsei Med J.*, 46 (2005) 585.
9. M. Soare, O. Păniță, C. Sălceanu, *Annals of the University of Craiova-Agriculture, Montanology, Cadastre Series*, XLV (2015) 300.
10. V. L. Singleton, J.A. Rossi, *Am. J. Enol. Vitic.*, 16 (1965) 144.
11. R. Soare, C. Babeanu, D. Bonea and O. Panita, *Scientific Papers-Series A, Agronomy*, 58 (2015) 307.
12. A. Paunescu, A. M. Dodocioiu, C. Babeanu, D. G. Buzatu, *Nano, Bio And Green – Technologies for a sustainable future Conference Proceedings, SGEM 2016, Book Series: International Multidisciplinary Scientific GeoConference-SGEM, Vol I* (2016) 437.
13. S. Enayat, S. Banerjee, *Food Chemistry*, 116 (2009) 23. O
14. F. F. Tavakoli, F. Rahmani, R. Heidari, *Current Nutrition & Food Science*, 12 (2016) 241.
15. T. Nyman, R. Julkunen-Tiitto, *Phytochemistry*, 66 (2005) 2836.
16. X. Li, Z. Liu, X. Zhang, L. Wang, Y. Zheng, C. Yuan, G. Sun, *Molecules*, 13 (2008) 1530.
17. G. Ciobanu, S. Neamtu, *Annals of the University of Craiova, The Chemistry Series*, XLII (1) (2013) 43.
18. R.J. Nijveldt, E. van Nood, D. E. C. van Hoorn, P. G. Boelens, K. van Norren, P. A. M. van Leeuwen, *American Journal of Clinical Nutrition*, 74 (2001) 418.
19. I. S. Young, J.V. Woodside, *J. Clin. Pathol.*, 54 (2001) 176.

20. B. Halliwell, *Lancet*, 355 (2000) 1179.
21. C. Babeanu, A.M. Dodocioiu, *Annals of the University of Craiova-Agriculture, Montanology, Cadastre Series*, XLVII (2) (2017) 20.
22. C. Babeanu, M. Soare, M. Corneanu, M. Dragoi, *International Multidisciplinary Scientific GeoConference Surveying Geology and Mining Ecology Management, SGEM*, 17(61) (2017) 665.



Thermal Analysis of some Binuclear Bioactive Complexes Derived from an Aromatic Dialdehyde and L-Tryptophan

Research article

*Florina Ciolan**, *Anca Gănescu*

University of Craiova, Faculty of Sciences, Department of Chemistry, Calea Bucuresti, 107i,
Craiova, Romania

*E-mail: florina_ciolan@yahoo.com

Received: 04.10.2017 / *Accepted:* 06.11.2017 / *Published:* 22.12.2017

Abstract

The binuclear complex compounds of Ni(II), Co(II), Cu(II) and Mn(II) derived from 2,2'-(propane-1,3-diylidioxy)dibenzaldehyde and L-tryptophan were studied by thermal analysis. Thermogravimetric analysis results were in good agreement with the proposed composition of the complexes.

Keywords: dialdehyde, aminoacid Schiff base, binuclear bioactive complexes, thermal analysis

1. INTRODUCTION

Aminoacid Schiff bases and their first-row transition metal complexes were reported to exhibit biological activity [1].

The template synthesis and the characterization by elemental analyses, molar conductivity, IR and electronic spectra, magnetic susceptibility measurements of the binuclear complexes of Ni(II), Co(II),

Cu(II) and Mn(II) derived from the aromatic dialdehyde, 2,2'-(propane-1,3-diylldioxy) dibenzaldehyde (named also 1,3-bis(2'-formylphenyl)-1,3-dioxapropane), and L-tryptophan, were presented in a previous study [2]. The results of antimicrobial tests [2] indicated that the Cu(II) complex was the most active of these compounds.

The aim of the present study was to confirm, by thermogravimetric analysis results, the chemical structures proposed for these binuclear complexes.

2. MATERIALS AND METHODS

The binuclear complexes of Ni(II), Co(II), Cu(II) and Mn(II) derived from 2,2'-(propane-1,3-diylldioxy)dibenzaldehyde and L-tryptophan were prepared according to a procedure described in a previous study, by template condensation of the aromatic dialdehyde, L-tryptophan and metal acetate in methanolic medium [2]. All the complexes were obtained by template synthesis since any attempt to isolate the free Schiff base ligand was unsuccessful, because it is easily hydrolysed in contact with water.

These ones were denoted as follows: $[\text{Cu}_2\text{L}(\text{AcO})_2(\text{H}_2\text{O})_4]$ (1), $[\text{Ni}_2\text{L}(\text{AcO})_2(\text{H}_2\text{O})_4]$ (2), $[\text{Co}_2\text{L}(\text{AcO})_2(\text{H}_2\text{O})_4]$ (3), $[\text{Mn}_2\text{L}(\text{AcO})_2(\text{H}_2\text{O})_4]$ (4), where $\text{L}=(\text{C}_{39}\text{H}_{34}\text{N}_4\text{O}_6)^{2-}$.

The thermal analysis measurements (TG, DTG and DTA) of the metal (II) complexes were carried using a horizontal "Diamond" Differential/ Thermogravimetric Analyzer from Perkin Elmer Instruments in dynamic nitrogen atmosphere (150 mL min^{-1}), in the 20-800 °C temperature range, with the heating rate of 10 °C min^{-1} .

3. RESULTS AND DISCUSSIONS

The spectroscopic data (IR and UV-Vis electronic spectra), as well as elemental analyses, molar conductivity measurements and magnetic susceptibility determinations, presented in a previous study [2], support the proposed general structures of the studied compounds (Figure 1).

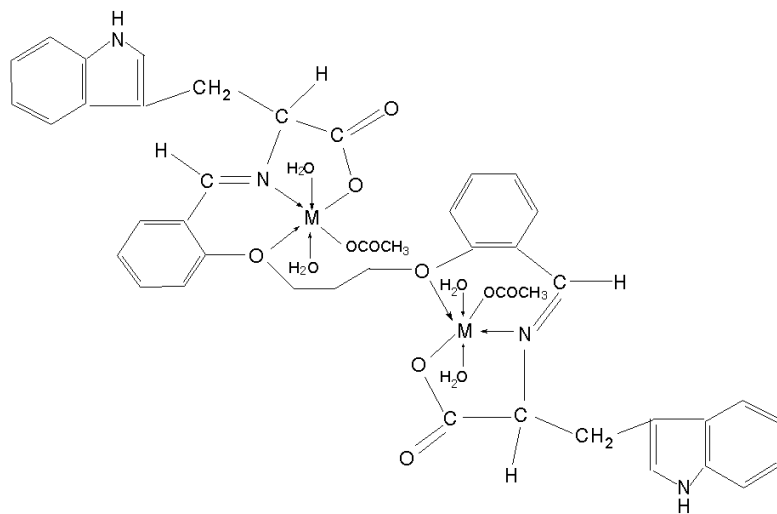
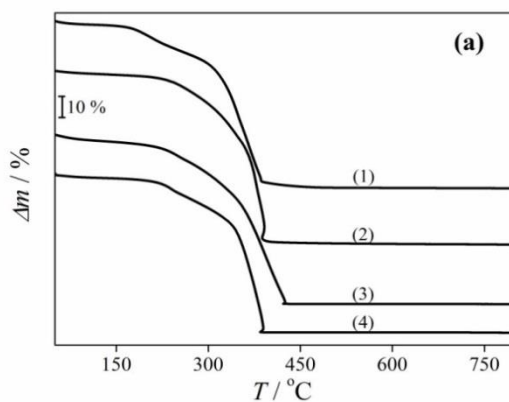


Figure 1. Proposed general structures of metal complexes derived from 2,2'-(propane-1,3-diylidioxy)dibenzaldehyde and L-tryptophan; M = Cu(II), Ni(II), Co(II) or Mn(II)

Thermal analysis of metal complexes is used to obtain information about their physical properties and thermal stability, as well as for the nature of the intermediates and final decomposition products [3-11].

In the temperature range 50-150 °C, the TG curves (Figure 2 (a)) of the complexes indicate a small mass loss (about 3-4 %), which can be attributed to the elimination of physically adsorbed water. This process is accompanied by a weak endothermic effect.



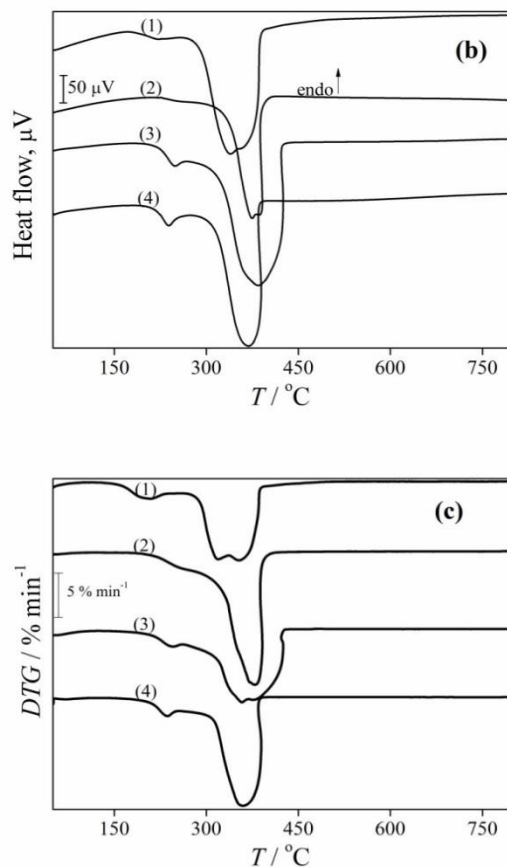


Figure 2. Thermal curves for metal complexes of Cu(II) – (1), Ni(II) – (2), Co(II) – (3) and Mn(II) – (4); **(a)** TG curves, **(b)** DTA curves, **(c)** DTG curves

The decomposition of all complexes started at 150°C and was completed at about 450-500 °C.

The TG and DTG curves (Figure 2 **(a)**, **(c)**) of the complexes decomposition indicate that the complexes (1) and (3) decompose in three steps, while the complexes (2) and (4) decompose in two steps and the final residual weight corresponds to the metal oxide.

Table 1 shows the thermogravimetric analysis results of the metal complexes decomposition.

Table 1. Thermogravimetric analysis data of the metal complexes

Complex	Temperature range, °C	Mass loss, %	Lost fragment	Residue, %
		exp. (calcd.)		exp. (calcd.)
(1)	150-220	7.10 (7.41)	4H ₂ O	2CuO 17.26 (16.37)
	220-341	30.10	2CH ₃ COO, fragments of L	
	341-500	45.54	fragments of L	
(2)	150-265	7.20 (7.48)	4H ₂ O	2NiO 15.23 (15.53)
	265-500	77.57 (76.92)	2CH ₃ COO, fragments of L	
(3)	150-250	7.20 (7.48)	4H ₂ O	2CoO 16.80 (15.57)
	250-360	27.36	2CH ₃ COO, fragments of L	
	360-450	48.64	fragments of L	
(4)	150-245	7.15 (7.54)	4H ₂ O	2MnO ₂ 21.64 (18.21)
	245-450	71.21 (74.18)	2CH ₃ COO, fragments of L	

The first step of decomposition for each metal complex, with a mass loss of about 7 %, could account for the loss of coordinated water [12, 13]. This decomposition step is accompanied by an exothermic effect (DTA curves- Figure 2 (b)) and this thermal behavior proves that the four water molecules are coordinated to the central metal ions [12]. Note that the removal of coordination water takes place at a lower temperature for complex (1) compared with all other complexes, indicating a weaker chemical bond.

The second step of decomposition for the complexes (2) and (4) may correspond to the loss of two coordinated CH₃COO groups [14] and of the organic part of these complexes (fragments of L), leaving corresponding metal oxide as residue (Table 1). This final step of decomposition is strongly exothermic.

For the complexes (1) and (3), the removal of two coordinated CH₃COO groups and of the organic part (fragments of L) takes place in

two slightly differentiated steps, as shown in Table 1. These last steps were also accompanied by a strong exothermic effect. In this case, the final residue is the corresponding metal oxide, too.

The thermogravimetric analysis results confirm the proposed general structures for the studied binuclear complexes (Figure 1).

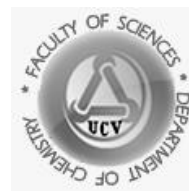
4. CONCLUSIONS

In this study, the binuclear bioactive complexes of Ni(II), Co(II), Cu(II) and Mn(II) derived from 2,2'-(propane-1,3-diylldioxy)dibenzaldehyde and L-tryptophan, obtained by template synthesis and characterized by various physico-chemical methods in a previous study, were studied by thermal analysis. Thermogravimetric analysis results are in good agreement with the proposed composition of the compounds and confirm the binuclear formulation of the $[M_2L(AcO)_2(H_2O)_4]$ type complexes, where M= Co(II), Ni(II), Cu(II) or Mn(II) and L= $(C_{39}H_{34}N_4O_6)^{2-}$.

References

1. S. Kumar, D. N. Dhar, P. N. Saxena, *Journal of Scientific & Industrial Research* 68 (2009) 181.
2. F. Ciolan, L. Patron, L. Marutescu, M. C. Chifiriuc, *Farmacia* 63(1) (2015) 86.
3. M. Badea, A. Emandi, D. Marinescu, E. Cristurean, R. Olar, A. Brăileanu, P. Budrugaec, E. Segal, *J. Therm. Anal. Cal.* 72 (2003) 525.
4. R. Olar, M. Badea, D. Marinescu, V. Lazar, C. Chifiriuc, *J. Therm. Anal. Cal.* 97 (2009) 721.
5. M. Badea, R. Olar, D. Marinescu, E. Segal, A. Rotaru, *J. Therm. Anal. Cal.* 88 (2007) 317.
6. R. Olar, M. Badea, N. Stănică, E. Cristurean, D. Marinescu, *J. Therm. Anal. Cal.* 82 (2005) 417.
7. A. Kropidłowska, A. Rotaru, M. Strankowski, B. Becker, E. Segal, *J. Therm. Anal. Cal.* 91 (2008) 903.

8. A. Rotaru, A. Kropidłowska, C. Constantinescu, N. Scărișoreanu, M. Dumitru, M. Strankowski, P. Rotaru, V. Ion, C. Vasiliu, B. Becker, M. Dinescu, *Appl. Surf. Sci.* 255 (2009) 6786.
9. A. Rotaru, C. Constantinescu, A. Mandruleanu, P. Rotaru, A. Moldovan, K. Gyoryova, M. Dinescu, V. Balek, *Thermochim. Acta* 498 (2010) 81.
10. M. Tătucu, P. Rotaru, I. Rău, C. Spînu, A. Kriza, *J. Therm. Anal. Cal.* 100 (2010) 1107.
11. P. Rotaru, R. Scorei, A. Hărăbor, M. Dumitru, *Thermochim. Acta* 506 (2010) 8.
12. B. Singh, P. C. Maurya, B. V. Agarwal, A. K. Dey, *J. Indian Chem. Soc.* 59 (1982) 29.
13. M. V. Patil, S. P. Malve, *J. Indian Chem. Soc.* 81 (2004) 683.
14. M. Sönmez, M. Şekerci, *J. Serb. Chem. Soc.* 72 (2007) 259.



Natural sources used to obtain edible films

Research articles

Mihaela Gabriela Dumitru

University of Craiova, Faculty of Sciences, Department of Chemistry, Calea Bucuresti, 107i,
Craiova, Romania

E-mail: dummg@yahoo.com

Received: 25.10.2017 / Accepted: 28.11.2017 / Published: 22.12.2017

Abstract

One of the more fashionable trends consists of the development of innovative biopolymers obtained from agricultural commodities and/or of food-waste products. The use of biopolymers in multiple food packaging applications has emerged as an alternative regarding their film-forming properties to produce edible films as an environmentally-friendly technology. Edible coatings can be made from a variety of polysaccharides. The objective of this work was to extract inulin from the bulbs of onions for use in obtaining edible polymers.

Keywords: Inulin, edible polymers

1. INTRODUCTION

Edible films are defined as a thin layer of material which can be consumed and provides a barrier to moisture, oxygen and solute movement for the food. The material can be a complete food coating or can be disposed as a continuous layer between food components [1, 2].

Edible films can be formed as food coatings and free-standing films, and have the potential to be used with food as gas aroma barrier [2, 3]. Edible films and coatings have received considerable attention in recent years because of their advantages over synthetic films. The main advantage of edible films over traditional synthetics is that they can be consumed with the packaged products.

These films can be produced from a variety of products, such as polysaccharides, proteins, lipids and resins, with or without the addition of other components (e.g. plasticizers and surfactants), Figure 1 summarizes a general scheme for the classification of edible films [4-6].

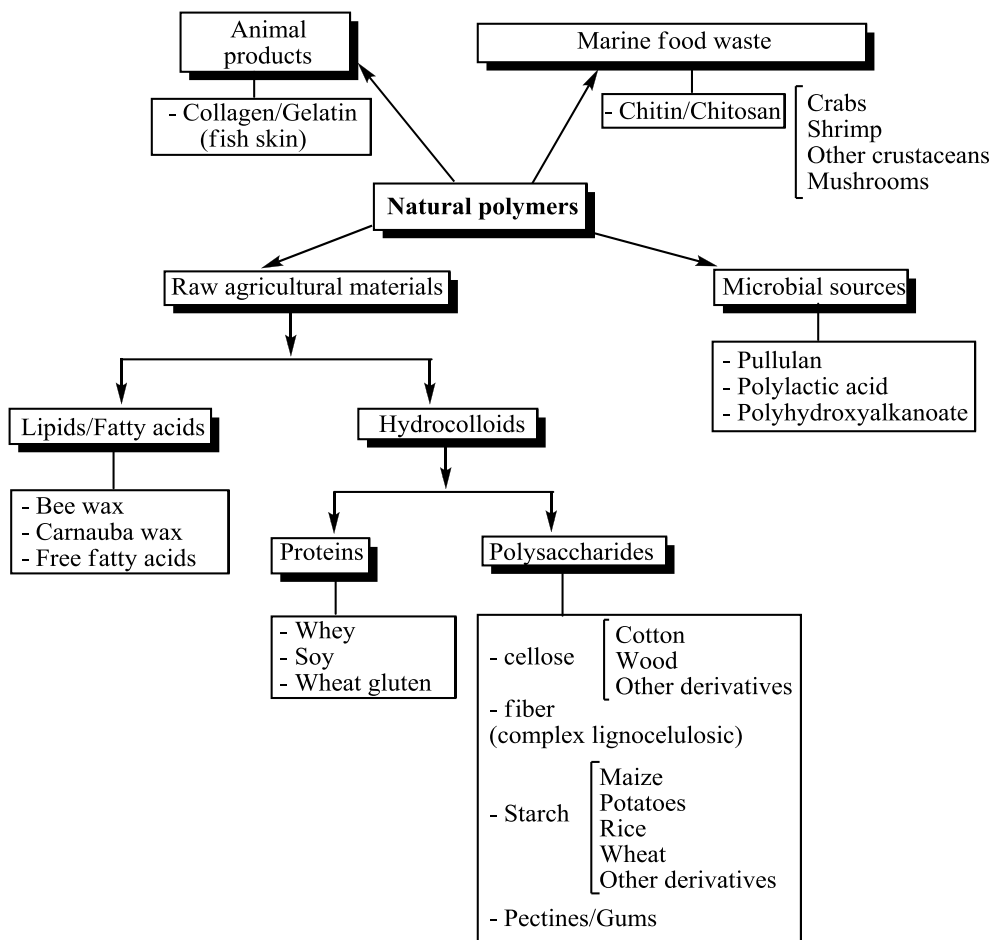


Figure 1. Sources of natural biopolymers

Chitin is probably the most abundant polysaccharide of nature after cellulose. It is also one of the most abundant biopolymer on the earth. It is found in fungi but principally among the arthropods (crabs and insects). Chitin (Figure 2) is closely related to cellulose. Here the alcoholic OH group on carbon atom 2 of β -D-glucose units is replaced by an N-acetylamino group. It is, thus, a linear polymer of N-acetyl-D-glucosamine units joined together by β -1, 4-glucosidic linkages. Chitin's pronounced stability is based on the hydrogen bonding of the N-acetyl side chains [7] Figure 2.

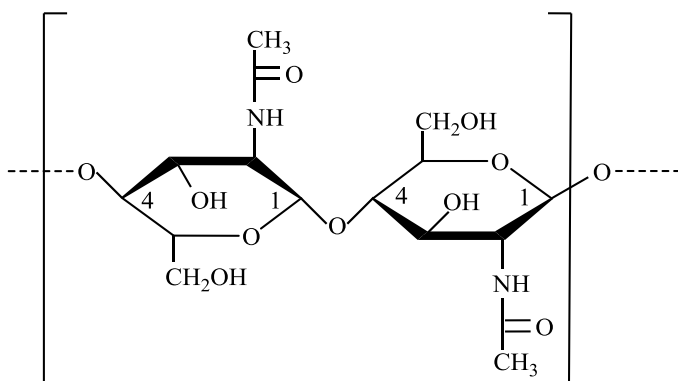


Figure 2. Molecular structure of Chitin

Pectin is a polysaccharide mixture with a complicated structure containing at least 65 % of galacturonic acid (GalA). Three structural elements are involved in the make-up of a pectin molecule: a homogalacturonan consisting of (1 \rightarrow 4) linked α -D-GalA, a galacturonan with differently arranged side chains (building blocks: apiose, fucose, arabinose, xylose), and a rhamnogalacturonan with a backbone consisting of the disaccharide units [\rightarrow 4)- α -D-GalA-(1 \rightarrow 2)- α -L-Rha-(1 \rightarrow)] and with its rhamnose residues linked by arabinan and galactan chains [8], Figure 3.

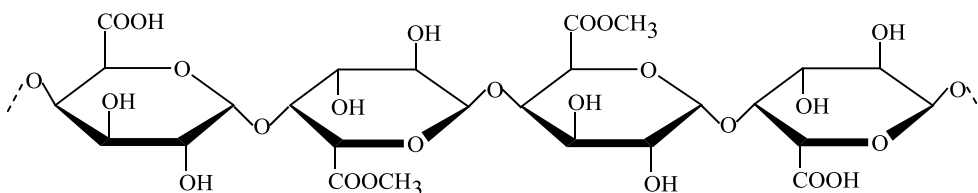


Figure 3. Molecular structure of Pectin

Pullulan is a polysaccharide polymer consisting of maltotriose units, also known as α -1,4- α -1,6-glucan'. Three glucose units in maltotriose are connected by an α -1,4 glycosidic bond, whereas consecutive maltotriose units are connected to each other by an α -1,6 glycosidic bond [9], Figure 4.

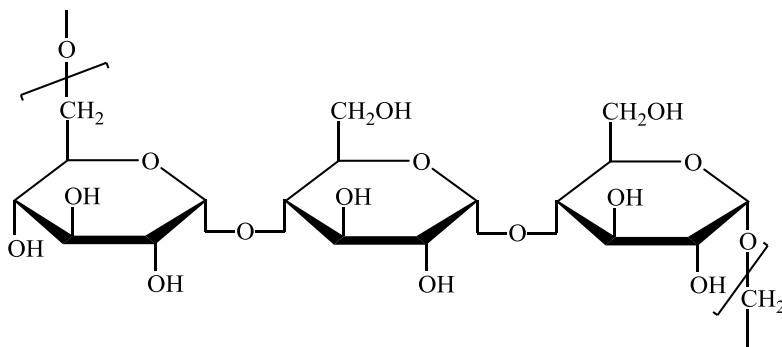


Figure 4. Molecular structure of Pullulan

Agar is a heterogenous complex mixture of related polysaccharides having the same backbone chain structure. The main components of the chain are β -D-galactopyranose and 3,6-anhydro- α -L-galactopyranose, which alternate through 1 \rightarrow 4 and 1 \rightarrow 3 linkages [8], Figure 5.

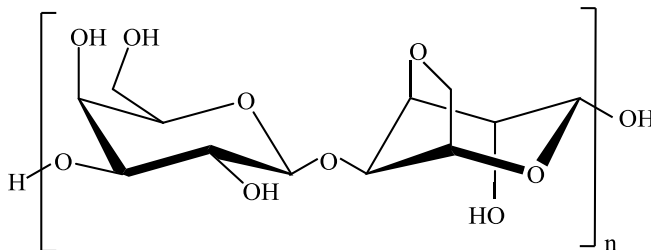


Figure 5. Molecular structure of Agar

Inulin is a polysaccharide, similar to starch, and exists as a white powder with neutral taste. Chemically, it is a linear biopolymer of D-fructose units connected by b (2,1) glycosidic linkages, and terminated with one D-glucose molecule linked to the fructose chain by an a (2,1) bond [10], Figure 6.

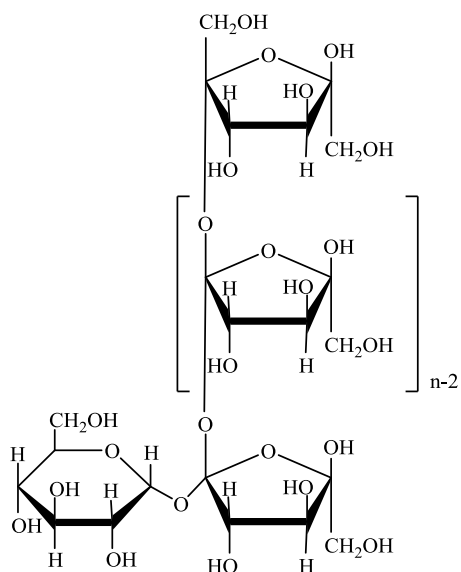


Figure 6. Molecular structure of Inulin

Table 1. The inulin content in vegetables, fruits and cereals

Source	Edible parts	Inulin content, % of fresh weight
Onion	Bulb	2-6
Jerusalem artichoke	Tuber Root	14-19 15-20
Chicory	Bulb	3-10
Leek	Bulb	0.3-0.7
Garlic	Leaves-	9-16
Artichoke	heart	3-10
Banana	Fruit	0.3-0.7
Rye	Cereal	0.5-1.5
Barley	Cereal	12-15
Dandelion	Leaves	3.5-4.0
Burdock	Root	12-22
Camas	Bulb	8-13
Murnong	Root	3-19
Yacon	Root	4-11
Salsify	Root	

Inulin is present in roots and rhizomes of a number of regularly consumed vegetables, fruits, and cereals, including leek, onion, garlic, wheat, chicory [11,12] and in a wide range of bacterial species [12-15], Table 1.

2. MATERIALS AND METHODS

2.1. Materials

Collection of Samples

The bulb onion were collected from a local market of Craiova, România.

Reagents and Chemicals

All analytical grade solvents, chemicals and acids used in the present study were obtained from different sources. The different reagents and chemicals used were: calcium hydroxide, oxalic acid, ethanol, acetone, hydrochloric acid, resorcinol.

2.2. Method

Extraction of inulin from onion

Samples of onion were washed with tap water to remove dust and other unwanted materials and grounded in a vertical blender Braun MR 404 Plus. In a reactor with a capacity of 2 L were introduced 800 mL distilled water and onion bulbs 400 g (ratio 2 : 1). The mixture was heated at 80 °C and permanently stirred for 3 h [16]. A Ca(OH)₂ solution was added until pH 8.0, and the mixture was left at room temperature for 1 h. The precipitated residue was filtered. The filtrate was neutralized (at t° = 60-65 °C) with oxalic acid to pH 7.0, a small amount of activated carbon was added, and the mixture was then stirred and filtered. The filtrate was left to cool down at 2-5 °C for 24 h. The precipitated amorphous mass was filtered through a Büchner funnel and rinsed twice with 95 % ethanol and once with acetone. It was dried at 40 °C [16].

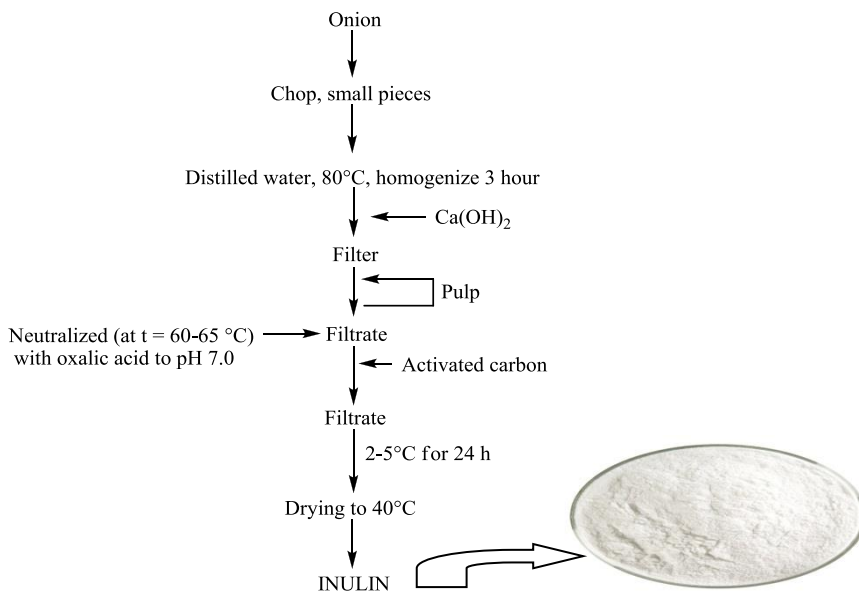


Figure 7. A flow chart of the inulin extraction process

Spectrophotometric method for determination of inulin:

2.0 cm³ of aqueous solution of inulin were mixed with 2.0 cm³ of 10 % HCl and heated for 10 min in a boiling water bath. 0.5 cm³ of Selivanov’s reagent (0.5 % solution of resorcinol in 20 % HCl) was added and further heated for 1 min. Absorption was measured at 520 nm. To plot a standard straight line (Figure 8), fructose and a spectrophotometer Carion -50 were used.

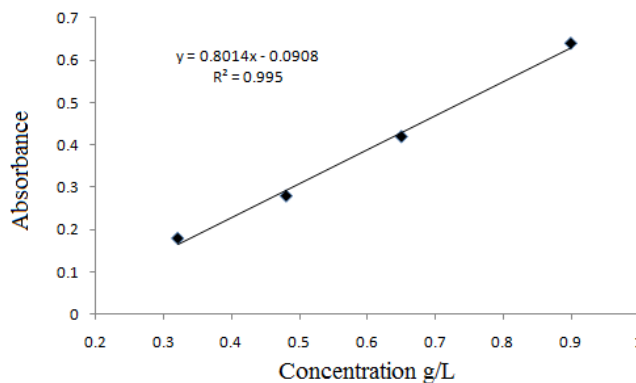


Figure 8. Fructose calibration curve

Solubility

The solubility of inulin was determined as follows: at 25 °C inulin was added slowly in 10 mL of water under stirring until complete dissolution and saturation. The solubility is expressed as the mass of inulin dissolved in one liter of distilled water [16].

Kinematic viscosity

A Ubbelohde type capillary viscometer with a 0.53-mm-diameter capillary was used.

The *kinematic viscosity*, was calculated according to the formula:

$$\nu = k \cdot t$$

where: k is the viscometer constant; t - the time (seconds) it takes for the liquid to pass through the two calibrated marks.

3. RESULTS AND DISCUSSION

After the process of extraction and measurement of inulin we found that onion contains 6 % inulin. The result is in concordance with other literature data [17, 18].

The solubility of the polymer film represents the dissolved dry matter content after a 24 hours immersion in water at 25 °C. The water solubility of the film is one of the major problems of polysaccharides films and it is determined through various methods: sorption and water activity, solubility, moisture content, permeability etc. The film solubility in water can also provide an insight about the behavior of a film in aqueous media, a measure of its resistance to water, and thus about the hydrophilicity of the related material. The moisture content is the parameter related to the total void volume occupied by water molecules in the film microstructure network. It is also an important factor when determining the film biodegradability when they are used as packaging materials. Sometimes, it is desired a high solubility in water. This is when the film or coating is consumed as food. The water solubility value of film was established to be 74 g L⁻¹ [19].

The viscosity of the polymers influences the process of forming the polymer film, its strength and drying time. The viscosity obtained for inulin extracted from the onion was 1.3 mm² s⁻¹.

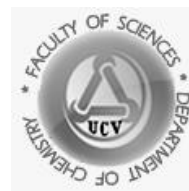
4. CONCLUSION

Food packaging, an important discipline in the area of food technology, concerns preservation and protection of all types of foods and their raw materials from oxidative and microbial spoilage. Edible films and coatings are thin layers of edible materials applied on food products that can play an important role on their preservation, distribution and marketing. These are produced from edible biopolymers and food-grade additives. Film-forming biopolymers can be proteins, polysaccharides or lipids. Onion is an important source for obtaining inulin required to use as a natural biopolymers.

References

1. S. Guilbert, *Food packaging and preservation*, Mathlouthi, M. Ed., London (1986).
2. T. Bourtoom, *Int. Food Res. J.*, (2008) 237.
3. J. J. Kester, O. R. Fennema, *Food Technol.*, 40(12) (1986) 47.
4. R. N. Tharanathan, *Trends Food Sci. Tech.*, 14(3) (2003) 71.
5. T. Mehdizadeh, T. Hossein, M. Seyed, R. Razavi, R. Abdol, *Veterinary Research Forum*, 3 (3) (2012) 167.
6. M. G. Dumitru, A. Ganescu, I. Dabuleanu, *Mater. Plast.*, Vol. 53 No.3, (2016) 414.
7. <http://www.cuchd.in>
8. H. D. Belitz, W. Grosch, P. Schierble, *Food chemistry*, 4th revised and extended Ed. Springer-Verlag Berlin (2009).
9. B. H. A. Rehm, *Microbial production of biopolymers and polymers precursors*, Ed., Caister Academic Press., Norfolk (2009).
10. L. Yang Q. S. He, K. Corscadden, C. C. Udenigwe, *Biotechnol. Rep.*, 5 (2015) 77.
11. M. B. Roberfroid, *Crit. Rev. Food Sci. Nutr.*, 33 (1993) 103.
12. F. Miremad, N. P. Shah, *Int. Food Res. J.*, 19(4) (2012) 1337.
13. I. Vijn, S. Smeekens, *Plant Physiol.*, 120 (1999) 351.
14. J. Van Loo, P. Coussement, L. DeLeenheer, H. Hoebregs & G. Smits, *CRC Crit. Rev. Food Sci. Nutr.*, 35 (1995) 525.

15. P. Denev, N. Delchev, G. Dobrev, Iv. Panchev, N. Kirchev, *Food Sci.*, 3 (2010) 48.
16. M. G. Dumitru, C. Teisanu, O. Gîngu, 4th International Conference: Advanced in Engineering & Management (ADEM), 17-18 Noiembrie, Turnu -Severin 2016. Conference book of abstracts. Ed. Universitaria Craiova, (2016) 13.
17. M. Sherif Abed, H. A. Abdelmoneim, N. Anwar, N. Sobia, A. Al-Farga, M. Bakry, *Int. J. Agric. Res*, 5(1) (1996) 2319.
18. L. De Leenheer, *Production and use of inulin: industrial reality with a promising future*, H. van Bekkum, H. Röper, F. Voragen Ed., New York (1996).
19. M. G. Dumitru, A. Gănescu, I. Dăbuleanu, *Mater. Plast.*,53(3) (2016) 414.



The oxidative dissolution of iron monosulfide (FeS): A Cyclic Voltammetry study

Research article

Mădălina Duinea^{1,2*}, *Maria Manea*¹, *Ana Sandu*¹, *Bianca Ghejan*¹, *Mihaela Petcu*¹, *Paul Chiriță*¹

¹University of Craiova, Department of Chemistry, Calea Bucuresti 107I, A.I. Cuza, Romania

²„Dunarea de Jos” University of Galați, Department of Chemistry, Physics and Environment, Domneasca Street 47, 800008- Galați, Romania

*E-mail: madalina.duinea@gmail.com

Received: 30.10.2017 / *Accepted:* 28.11.2017 / *Published:* 22.12.2017

Abstract

The oxidative dissolution of FeS leads to serious environmental problems, the most important being the acid mine drainage. Hence, the oxidative dissolution of FeS in acidic solutions (pH 2.15) and at a temperature of 27 °C was studied by Cyclic Voltammetry. It was found that at positive potentials both Fe²⁺ and S²⁻ are oxidized, while at negative potentials the oxidized sulfur is reduced to S²⁻. The addition of glycine to the reaction system produced a narrow passivation plateau at approximately -0.3 V. The initial and reacted surfaces were analyzed by optical microscopy. The reacted surface reveals the presence of Fe(III) oxyhydroxides.

Keywords: FeS, Oxidative dissolution, Cyclic Voltammetry, Optical microscopy.

1. INTRODUCTION

The mining industry has an important contribution to the economic development of many countries from around the world. Unfortunately, it produces serious environmental problems, the most harmful being the acid mine drainage (AMD) [1-5]. AMD is characterized by low pH (1-4), high electrical conductivity, extremely high concentrations of Fe^{3+} and SO_4^{2-} , and the presence of other elements toxic or potentially toxic to the environment (Cu, Zn, Al, Hg, As, Pb, Cd, Co, Cr, Ni) [3-5].

Iron monosulfide phases are known to be the most reactive iron sulfides. Their reactivity is one of factors which contribute to the production of AMD. It was experimentally demonstrated that the presence of some organic compounds in the reaction system leads to the decrease of the iron sulfides oxidative dissolution and implicitly the diminution of the intensity of this phenomenon [2, 5-7].

The aim of this study is the investigation of FeS oxidative dissolution in acidic solutions (pH 2.15) of 0, 0.02 or 0.04 mM glycine, at a temperature of 27 °C. The behavior of FeS was characterized by Cyclic Voltammetry and optical microscopy.

2. MATERIALS AND METHODS

The electrochemical experiments were carried out with the electrochemical workstation Zahner Zennium connected to a classic electrochemical cell with three electrodes, filled with experimental solutions of glycine (0, 0.02 or 0.04 mM) at pH 2.15 and a temperature of 27 °C. The data were recorded with the specialized Thales program. The working electrode was made with the Buehler Isomet equipment from synthetic FeS. Its exposed surface was 1 cm².

The electrode has polished with SiC grinding paper (600 to 1200), washed with acetone and ultrasonicated for 10 minutes in ethyl alcohol. At the end of the experiments the surface of electrodes was washed with distilled water, dried and then examined with an optical microscope

(KRUSS, A.Kruss Optronic, Germany) using two different lenses (40x and 100x).

3. RESULTS AND DISCUSSION

3.1. Cyclic Voltammetry

The Cyclic Voltammograms of the FeS electrode in the absence and, respectively, the presence of glycine ($[\text{glycine}] = 0.02$ or 0.04 mM) are shown in Figure 1. Experiments of the Cyclic Voltammetry were carried out on the potential interval from -1 V to 1 V with a scan rate of 100 mV s^{-1} . Analyzing Figure 1 it can be observed that the Cyclic Voltammograms are very simple. Practically, the rate of the oxidation and respectively reduction processes linearly vary with the applied potential. At positive potentials both iron (Fe^{2+}) and sulfur (S^{2-}) from FeS are oxidized, while at negative potentials the oxidized sulfur species are reduced to S^{2-} . In the presence of 0.02 mM glycine the anodic current densities increase whereas the extreme cathodic current densities decrease when are reported at the current densities of FeS electrode in the absence of glycine or in the presence of 0.04 mM glycine.

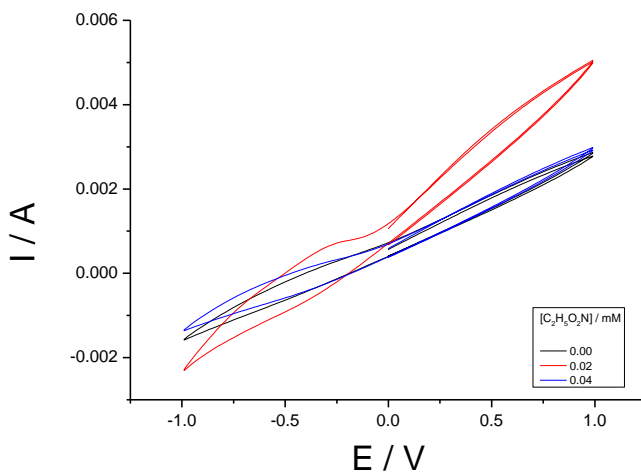


Figure 1. Cyclic Voltammograms of FeS electrode in the absence and, respectively, the presence of glycine ($[\text{glycine}] = 0.02$ or 0.04 mM) at pH 2.15 and 27 $^{\circ}\text{C}$

3.2. Optical microscopy

The surface of FeS electrode was analyzed with an optical microscope. For this purpose, two different lenses were used in order to observe the modifications that appeared after the electrochemical experiments.

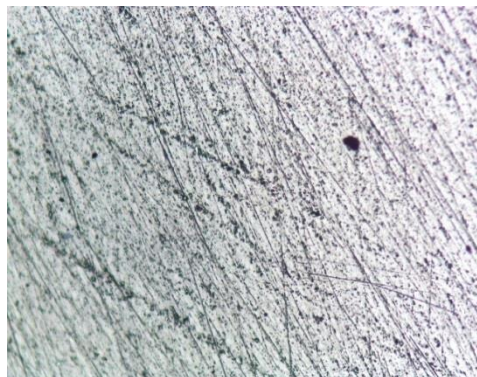


Figure 2. Initial surface of FeS (40x)

In Figure 2 is shown the initial surface of the electrode. The traces of polishing (visible in Figure 2) disappeared after the experiment performed in the absence of glycine, and small colored areas appeared (Figure 3). These areas can be associated with the appearance of the oxidation products (most probable Fe(III) oxyhydroxides) [7].

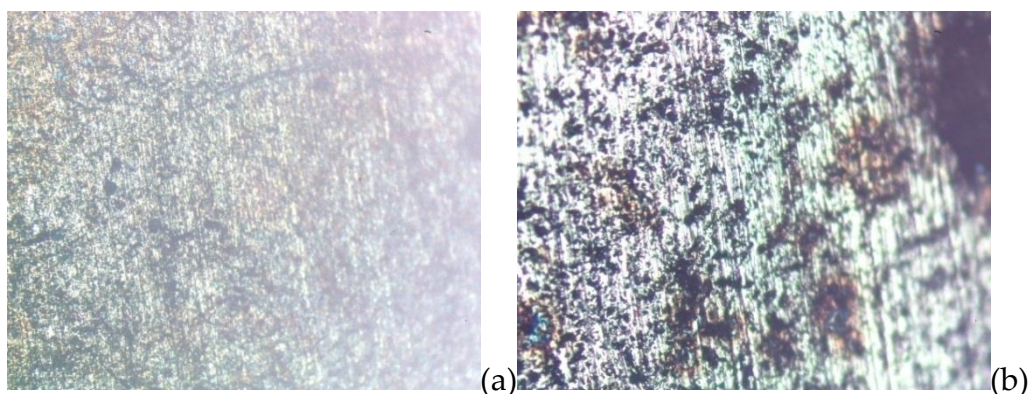


Figure 3. FeS electrode surface after the electrochemical experiments in the absence of glycine analyzed with the lenses 40x (a) and 100x (b)

The electrode surface after the experiments carried out in the presence of glycine (0.02 or 0.04 mM) was also analyzed. The obtained images are shown in Figure 4 ([glycine]=0.02 mM) and, respectively, Figure 5 ([glycine]=0.04 mM).

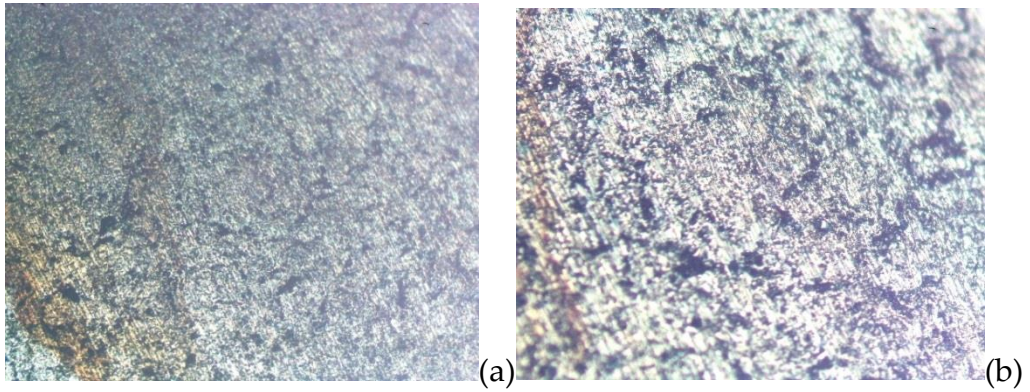


Figure 4. FeS electrode surface after the electrochemical experiments in glycine solution of 0.02 mM analyzed with the lenses 40x (a) and 100x (b)

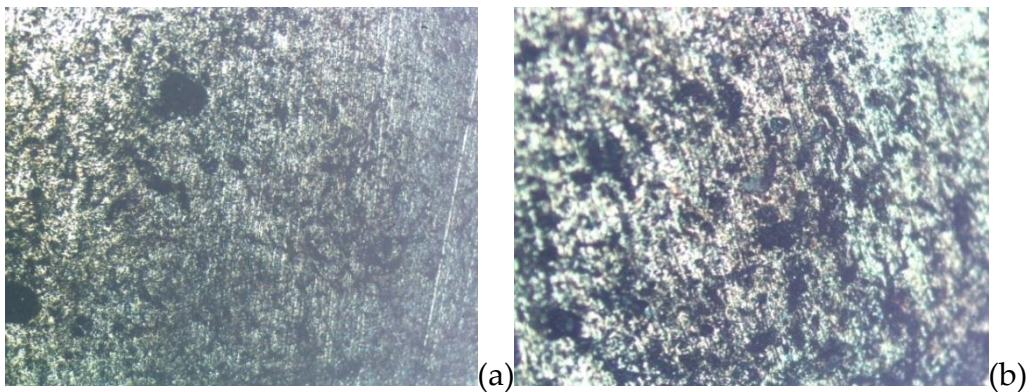


Figure 5. FeS electrode surface after the electrochemical experiments in glycine solution of 0.04 mM analyzed with the lenses 40x (a) and 100x (b)

As in the case of the experiment carried out in the absence of glycine, the polishing traces present on the initial surface of the electrode disappeared. The resulted surface is corroded and reveals

smaller amounts of oxidation products than the surface presented in Figure 3. The obtained microscope images are in good concordance with the results of Cyclic Voltammetry.

4. CONCLUSIONS

The oxidative dissolution of FeS in acidic solutions (pH 2.15) and at a temperature of 27 °C was studied by Cyclic Voltammetry. At positive potentials both Fe²⁺ and S²⁻ are oxidized, while at negative potentials the oxidized sulfur species are reduced to S²⁻. The presence of 0.02 mM glycine produces the increase of the anodic current densities and the decrease of the extreme cathodic current densities relative to the current densities determined in the absence of glycine or in the presence of 0.04 mM glycine. The initial and reacted surfaces were analyzed with an optical microscope. From the analysis of reacted surfaces, it was observed the presence of Fe(III) oxyhydroxides.

Acknowledgements

This work was supported by a grant of the Romanian National Authority for Scientific Research, CNDI–UEFISCDI, project number 51/2012.

References

1. V. Oros, *Biotehnologii de preparare a substantelor minerale utile. Biotehnologia metalelor*. Editura Universitatii de Nord Baia Mare, (1999).
2. P. Chiriță, C. A. Constantin, C. E. Badica, M. I. Duinea, L. M. Birsa, E. Matei, I. Baltog, *Mater. Chem. Phys.*, 157 (2015) 101.
3. P. Acai, E. Sorrenti, T. Gorner, M. Polakovic, M. Kongolo, P. de Donato, *Colloids Surf. Physicochem. Eng. Asp.*, 337 (2009) 39.
4. M. F. Cai, Z. Dang, Y. W. Chen, N. Belzile, *Chemosphere.*, 61 (2005) 659.

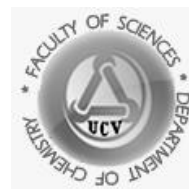
5. M. Simon, F. Martin, I. Ortiz, I. Garcia, J. Fernandez, E. Fernandez, C. Dorronsoro, J. Aguilar, *Sci. Total Environ.*, 279 **(2001)** 63.
6. C. A. Constantin, P. Chiriță, C. E. Badica, L. M. Birsa, E. Matei, I. Baltog, M. L. Schlegel, *Book of abstracts. 23rd Annual V.M. Goldschmidt Conference Florence*, **(2013)** 911.
7. C. E. Badica, M. I. Duinea, L. M. Birsa, M. A. Baibarac, E. Matei, P. Chiriță, *Book of abstracts. 24th Annual V.M. Goldschmidt Conference Sacramento*, **(2014)** 95.

Annals of the University of Craiova

The Chemistry Series

Volume XLIV, No. 2 (2017) 82-90

homepage: chimie.ucv.ro/anale/



Synthesis and description of three square-planar d^8 complex compounds involving charge-transfer systems

Research article

Liana Simona Sbîrnă^{1*}, *Clementina Moldovan*²

¹University of Craiova, Faculty of Sciences, Department of Chemistry, Calea București, 107i, Craiova, Romania

²University of Petroșani, Faculty of Mining, Department of Management, Environmental Engineering and Geology, Strada Universității, 20, Petroșani, Romania

*e-mail: simona.sbirna@gmail.com

Received: 29.11.2017 / Accepted: 18.12.2017 / Published: 22.12.2017

Abstract

The paper presents the synthesis and the characterization of three charge-transfer complex compounds of the $[M-S_2N_2]$ type, formed by d^8 transition metal ions – namely Ni(II), Pd(II) and Pt(II) – with a bidentate ligand of the naphthoquinone series.

The structural study of these three complex compounds was conducted by using elemental analysis, polarographic measurements, magnetic susceptibility and electric conductivity investigations, together with the results obtained from the IR and UV-Vis spectra.

Keywords: bidentate ligands, naphthoquinone derivatives, d^8 metal ions, square-planar complex compounds, charge-transfer systems

1. INTRODUCTION

Various references report data regarding different complex compounds formed by transition metal ions with ligands having conjugated double bonds, *i.e.*, systems of delocalized electrons in their molecules [1-4].

These combinations are square-planar, no matter the oxidation state of the metal ion.

The special interest provoked by these complexes is due, among others, to the fact that the complex compounds readily participate in reversible charge-transfer reactions:

$$[M-X_2Y_2]^{2-} \rightleftharpoons [M-X_2Y_2]^- \rightleftharpoons [M-X_2Y_2]^0 \rightleftharpoons [M-X_2Y_2]^+ \rightleftharpoons [M-X_2Y_2]^{2+}$$

where $X = Y = S$; $X = Y = O$; $X = Y = N$; $X = O, Y = S$; $X = O, Y = N$; $X = S, Y = N$ (the latter being the case hereby studied).

Within this work we have used a naphthoquinonic derivative as bidentate ligand: 2-thio-3-nicotinamido-1,4-naphthoquinone (which will be denoted as LH in what follows).

2. MATERIALS AND METHODS

2.1. Materials

The main chemicals that we have used were: $NiCl_2 \cdot 6H_2O$ (Merck, a.p.), aqueous solution (0.02M); $PdCl_2$ (BDH, a.p.), aqueous solution (0,02M); $K_2[PtCl_4]$ (BDH, a.p.); (0.02M); 2-thio-3-nicotinamido-1,4-naphthoquinone (double recrystallized), dimethylformamidic solution (0.02M). We also used tetrabutylammonium perchlorate, ethanol, diethyl ether, DMF and acetone, all these chemicals being of analytical purity as well.

The elemental analysis was performed on a Perkin Elmer 2380 (USA) instrument. The magnetic susceptibilities of these three complex compounds were investigated with a Holmarc Gouy's Method Apparatus, Model HO-ED-EM-08 (India), whereas their electrical conductivities were measured on a Radelkis OK-102/1 (Hungary) conductivity meter with a cell constant of $0,9 \text{ cm}^{-1}$, in 10^{-4} M DMF

solutions, at 23 °C. The polarograms were recorded with a Model 7-77-4/b Orion KTS polarograph, measuring the half-wave potentials at room temperature, using a calomel reference electrode together with a dropping mercury measuring electrode and a 10^{-1} M solution of tetrabutylammonium perchlorate as supporting electrolyte; the solutions of the complexes were all 10^{-3} M. The IR spectra were recorded on a Perkin Elmer FT-1600 Hewlett Packard analyzer, in anhydrous KBr pellets, whereas the electronic spectra were realised by using an Ocean Optics (UK) spectrophotometer, in 10^{-3} M acetone solutions.

2.2. Methods

The preparation of the heterocyclic ligand (2-thio-3-nicotinamido-1,4-naphthoquinone, denoted as LH in what follows) was presented elsewhere [5].

The complex compounds formed by Ni(II), Pd(II) and Pt(II) with it have been prepared by following the classical procedure described by Jensen and Nielsen [6].

More precisely, the nickel compound has been obtained by adding DMF solution of ligand to aqueous solution of nickel dichloride in a 2:1 molar ratio. After settling for an hour, the formed precipitate has been filtered on a G_4 porosity glass filter, washed with absolute ethanol, then with diethyl ether and finally dried under reduced pressure. The other two complexes were prepared using similar methods.

3. RESULTS AND DISCUSSION

3.1. Preliminary statements

All the complexes are air-stable, having the melting points higher than that of the ligand (their values are presented in Table 1, among other properties and together with the results of the elemental analysis).

Table 1. Properties and results of the elemental analysis

[ML ₂]	Mol wt. calcd	m.p. (°C)	Molar conductivity (W ⁻¹ cm ² mol ⁻¹)	Magnetic susceptibility (BM)	Elemental analysis (%)		
						Calcd	Found
[NiL ₂]	676.71	123	2.98	0	Ni	8.68	9.02
					C	56.75	56.89
					S	9.46	9.22
					N	8.28	8.07
					H	2.66	2.84
[PdL ₂]	724.4	158	1.44	0	Pd	14.69	14.75
					C	53.01	53.32
					S	8.83	8.49
					N	7.73	7.27
					H	2.48	2.85
[PtL ₂]	813.09	169	2.88	0	Pt	22.99	22.65
					C	47.22	47.56
					S	7.87	7.67
					N	6.89	6.59
					H	2.21	2.43

3.2. Appearance and solubility

The nickel complex is a microcrystalline stable red powder exhibiting low solubility in common organic and inorganic solvents. The other two are also microcrystalline stable powder with low solubility in usual organic and inorganic solvents, only the color being different (orange for the palladium compound and yellowish for the platinum one).

3.3. Polarographic measurements and interpretation

The study regarding these three complex compounds was completed with polarographic determinations. There are three polarographic half-wave potentials in the polarograms of all studied compounds. This fact proves the existence, in solution, of several

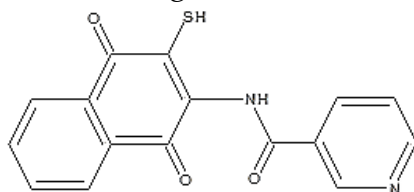
reduced species. It also shows that the reduction of the neutral and monoanionic species takes place at the dropping mercury electrode:



The other observed waves are due to the reduction of the ligands. The data gathered in assembly with these complexes demonstrate that, apart from representing a charge-transfer system, each of the evidenced species can also be chemically obtained, because the half-wave potentials range between +0.95 V and -0.95 V, which is a region where oxidizing or reducing agents do not disintegrate the complex compound.

3.4. Assumed structural formula for the complex compounds and explanation

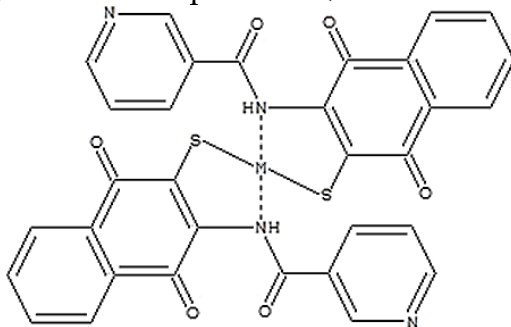
The structure of the free ligand is the one shown below.



2-thio-3-nicotinamido-1,4-naphthoquinone (denoted as LH)

The elemental analysis has shown that the complex compounds contain (besides the metal ion) two molecules of organic ligand. This statement is sustained by the spectral analysis, as proved in what follows.

Subsequently, the structure of the complex compound, suggested by the preliminary facts earlier presented, seems to be the one below:



$[M(II)L_2]$, where $M = Ni / Pd / Pt$

The reason for the notation LH becomes clear in this point of discussion, observing that one hydrogen atom of the bidentate ligand was lost as a consequence of complexation.

A confirmation about the type of the atoms involved in the coordination and the nature of chemical bonds (proving that this assumption is correct) was achieved based on the infrared spectra and electronic spectra performed for the free ligand and the three complex compounds. The wavenumbers thus obtained for all the compounds discussed here are labeled in Table 2.

Table 2. IR spectral data for the ligand and complexes ($\tilde{\nu}$ are expressed in cm^{-1})

Comp.	$\tilde{\nu}_{\text{NH}}$	$\tilde{\nu}_{\text{CO}}$	$\tilde{\nu}_{\text{CN}}$ coupl C-C	$\tilde{\nu}_{\text{CN}}$ coupl .NH ₂	$\tilde{\nu}_{\text{CS}}$	$\tilde{\nu}_{\text{ske}}$ C=C	$\tilde{\nu}_{\text{CH}}$ plan e def.	$\tilde{\nu}_{\text{NH}}$	$\tilde{\nu}_{\text{CS}}$
LH	3482 i 3370 i	1670 i	1580 i	1356 i	1210 i	1150 m	1005 w	755 vi	670 m
[NiL ₂]	3410 w 3304 w	1672 i	1585 m	1355 m	1258 w	1145 m	1006 w	758 vi	678 w
[PdL ₂]	3415 sh 3308 w	1675 i	1590 w	1358 m	1265 sh	1148 m	1008 w	760 vi	675 sh
[PtL ₂]	3412 w 3306 sh	1673 i	1585 sh	1360 m	1253 w	1143 m	1007 w	756 i	673 sh

vi = very intense; i = intense; m = medium; w = weak; sh = shoulder.

The infrared spectra show important changes between 3500 cm^{-1} and 3000 cm^{-1} , a region including characteristic vibrations of the $-\text{NH}_2$ group. This shows that the nitrogen atoms are directly involved in the coordination process. Moreover, the intense bands in the $1600\text{-}1300 \text{ cm}^{-1}$ range ($\tilde{\nu}_{\text{C-N}}$, coupling C-C and $\tilde{\nu}_{\text{C-N}}$, coupling NH₂), appear in the complex compounds at slightly modified wavenumbers and with diminished intensities.

An argument that supports the participation of the sulfur atom to the coordination is the change of the intense band at 1210 cm^{-1} , which expresses an important alteration of the C=S bond during the

coordination (in the complex compounds it suffers, indeed, an important decrement in intensity). Another argument is the modification occurring in the 680-630 cm^{-1} band, generally assigned to the C=S vibration, which is moved, in the complexes, also appearing with a much lower intensity.

Finally, in order to establish the real coordination geometry of these complex compounds, a spectral analysis in the UV-Vis range was performed. Although the symmetry point group is not D_{4h} , but D_{2h} , the bands observed in the electronic absorption spectra of the studied complexes might be assigned according to the classical paths followed by Gray and Ballhausen [7] and Vanquickenborne [8].

Table 3. UV-Vis spectral data for the complexes ($\tilde{\nu}$ are expressed in cm^{-1})

[ML ₂]	$\tilde{\nu}$	ϵ
[NiL ₂]	20513	0.75
	29151	0.34
	32712	0.25
	37236	0.57
[PdL ₂]	16817	0.53
	21342	0.48
	30623	0.25
[PtL ₂]	21682	0.38
	26323	0.42
	30348	0.23

The correspondence between the bands in the prepared complexes and the bands described for the typical complexes of the type [MX₂Y₂] leads to the assumption that all these new compounds have the same square-planar geometry. The D_{4h} - D_{2h} correlation assignment of the bands was reported elsewhere [9].

In the nickel complex, the first absorption band is assigned to an electron transfer localized on the sulfur atom to the transition metal ion and the second one is assigned to an electron transfer localized on the nitrogen atom. These transitions are shifted toward higher wavenumbers for the coordinated ligands, just as a consequence of the coordination. The shifts are caused by the mixing of the antibonding orbitals with d -

metal orbitals, as well as to the decrease in energy that occurs or the electron lone pairs after coordination. The last two bands are due to transitions between molecular orbitals practically localized on the oxygen atoms of naphthoquinone.

By comparing the spectra of the complex compounds with the one of the free organic ligand, it shows that the first two bands are shifted, while the last two ones are unshifted, meaning that the oxygen atoms have nothing to do with the coordination, which is realised by means of the sulfur and nitrogen atoms of the two identical ligand molecules [9]. Similar interpretation might be conducted for the palladium and platinum complexes.

4. CONCLUSION

As a conclusion to all the data gathered and then interpreted, one can state that the proposed structural formula is the real one for the complex compound of nickel, and then, similarly, for the other two complex compounds. The correlation of the elemental chemical analyses with the results of the physico-chemical determinations suggest that the complexes described in this paper are all of the type $[M-N_2S_2]$, where $M = Ni(II), Pd(II), Pt(II)$. This formulation is supported by the IR spectral analyses, which confirm that 2-thio-3-nicotinamido-1,4-naphthoquinone act as bidentate ligands having both nitrogen and sulfur as donor atoms. Finally, the electronic spectra of the studied complexes lead to the conclusion that they are square-planar. Polarography data prove their involvement in the electron-transfer processes.

The reason for the notation LH becomes clear in this point of discussion, observing that one hydrogen atom of the bidentate ligand was lost as a consequence of complexation.

References

1. N. Li, F. L. Zeng, Y. Wang, D. Z. Qu, *Chinese Journal of Polymer Science* (2017) <https://doi.org/10.1007/s10118-018-2014-1>.
2. D. Chen, D. Wang, Z. Xiao, H. Wang, K. Yang, *Bioprocess and Biosystems Engineering* (2017) <https://doi.org/10.1007/s00449-017-1879-7>.
3. B. Dúzs, I. Szalai, *Reaction Kinetics, Mechanisms and Catalysis* (2017) <https://doi.org/10.1007/s11144-017-1329-1>.
4. M. F. Budyka, T. N. Gavrishova, O. D. Laukhina, *Russian Chemical Bulletin* 44 (1995) 1656. <https://doi.org/10.1007/BF01151286>.
5. N. Mureşan, L. S. Sbîrnă, S. Sbîrnă, V. Mureşan, C. I. Lepădatu, *J. Ind. Chem. Soc.*, 79(5) (2002) 412.
6. K. A. Jensen, P. H. Nielsen, *Acta Chemica Scandinavica*, 20 (1966) 597.
7. H. P. Gray, C. J. Ballhausen, *J. American Chem. Soc.*, 85 (1963) 260.
8. L. G. Vanquickenborne, *Inorg. Chem.*, 20 (1981) 796.
9. V. Mureşan, L. S. Sbîrnă, S. Sbîrnă, C. I. Lepădatu, N. Mureşan, *Acta Chimica Slovenica*, 49(3) (2002) 447.